DEPLETED TO REFERTILIZED MANTLE PERIDOTITES HOSTING CHROMITITES WITHIN THE TUNCELI OPHIOLITE, EASTERN ANATOLIA (TURKEY): INSIGHTS ON THE BACK ARC ORIGIN

Okay Çimen[*,°,✉], **Fatma Toksoy-Köksal**[*], **Ayten Öztüfekçi-Önal**[**] and **Alican Aktağ**[*,°]

* *Department of Geological Engineering, Middle East Technical University, Ankara, Turkey.*
** *Department of Metallurgical and Materials Engineering, Tunceli University, Turkey.*
° *Department of Geological Engineering, Tunceli University, Turkey.*
✉ *Corresponding author, email: cokay@metu.edu.tr*

Keywords: *chromitite, peridotite, petrogenesis, back arc basin. Tunceli, Eastern Anatolia.*

ABSTRACT

The Tunceli Ophiolite, which represents the eastern part of the Izmir-Ankara-Erzincan Suture Belt (IAESB), hosts several chromite mines. The petrological characteristics of these deposits and their host rocks were investigated here for the first time. This ophiolite includes serpentinized peridotites, harzburgites, dunites, gabbros, sheeted dykes, pillow lavas and mudstones. The chromite occurrences are hosted in the mantle peridotites. The spinel group minerals in the ore and in ultramafic samples were sampled in seven different chromite mines (Yıldırım, Aksu, Hasangazi, Atilla, Eskigedik, Işıkvuran and Oymadal). The chromitite spinels display podiform characteristics. The Cr# = (0.39-0.89) and Mg# = values (0.43-0.74) of these spinel group minerals mainly correspond to magnesiochromite and chromite compositions. The silicate assemblage of the cpx-poor harzburgites include Mg-rich olivine (Fo_{91}), enstatite and diopside. The occurrence of Ti-enriched secondary clinopyroxenes likely reflect refertilization processes which may have originated by interaction between Ti-rich melts and highly depleted peridotites. The average Cr_2O_3 (15.46 %wt) and ΣPGE (92.10 pbb) contents of the chromitites from the Tunceli ophiolite are lower than those of other chromitite-bearing ophiolites in Turkey. The consistent geochemical and mineral chemistry data from the mantle peridotites and chromitites within the Tunceli Ophiolite suggest formation in an intra-oceanic back-arc basin which may have been active during the closure of northern branch of the Neotethyan ocean.

INTRODUCTION

Petrological features of the mantle peridotites and chromitites provide significant informations to unravel mantle sources and geodynamic evolution of the oceanic lithosphere (Zhou and Robinson, 1997; Pearce et al., 2000; Barnes and Roader, 2001; Zaccarini et al., 2005; 2011; Ghazi et al., 2011; Garuti et al., 2012; Montanini et al., 2012; Saccani et al., 2013; Saccani and Tassinari, 2015; Sanfilippo et al., 2015). Moreover, chromite deposits are economically major source of chromium and platinum group elements (PGEs, Uysal et al., 2007). In Anatolia, mantle bodies including chromite deposits have been mostly studied in terms of their petrological and economic characteristics (e.g., Akbulut et al., 2010; Uçurum et al., 2000; Uysal et al., 2005; 2007; 2009).

Anatolia was formed by assemblage of several terranes or continental micro-plates during the closure of the Neotethyan oceanic branches (e.g., Şengör and Yılmaz, 1981; Göncüoğlu et al. 1997, 2006a; Aldanmaz et al., 2008; Robertson et al., 2013). The İzmir-Ankara-Erzincan Suture Belt (IAESB), which stretches from the Aegean Sea to the Lesser Caucasus, is located between the Anatolide-Tauride Platform (ATP) in the south and the Sakarya Composite Terrane (SCT) in the north (Göncüoğlu et al., 2000). This suture belt includes remnants of the Northern Neotethys (Fig. 1a) and comprises ophiolitic sheets and ophiolite-bearing mélanges. They have been derived from a complex subduction-accretion system during the closure of the Neotethyan ocean (Şengör and Yılmaz, 1981; Okay and Şahintürk, 1997; Aldanmaz et al., 2008).

The ages of the ophiolites range from Late Jurassic to Early Cretaceous (Dilek and Thy, 2006; Topuz et al., 2013), whereas formation of the mélange was assigned to Late Cretaceous (e.g., Yılmaz et al., 1997; Okay et al., 2006; Parlak et al., 2012; Robertson et al., 2013). The geochemical characteristics of the ophiolites suggest different tectonic setting such as mid-ocean ridge, oceanic island, island arc and back-arc basin (e.g., Yalınız et al., 2000; Toksoy-Köksal et al., 2001; 2009; Göncüoğlu et al., 2006a; 2006b; Aldanmaz et al., 2008; Parlak et al., 2012). Their emplacement onto the Tauride-Anatolide margin started in the Maastrichtian, and lasted until Early Eocene (Şengör and Yılmaz, 1981; Yılmaz et al., 1997; Floyd et al., 2000; Göncüoğlu et al., 2000).

The İzmir-Ankara (Floyd, 1993; Önen and Hall, 1993; Yalınız et al., 2000; Floyd et al., 2000; Göncüoglu et al., 2000; Toksoy-Köksal et al., 2001; 2009; Önen, 2003; Göncüoğlu et al., 2006b; Aldanmaz et al., 2008; Bortolotti et al., 2013) and Ankara-Erzincan (Şengör and Yılmaz, 1981; Okay and Şahintürk, l997; Yılmaz et al., l997; Dilek and Thy, 2006; Rice et al., 2006; Eyüboğlu et al., 2007; Çelik et al., 2011; Parlak et al., 2012; Topuz et al., 2013; Robertson et al., 2013) parts of this suture belt have been extensively investigated. However, the ophiolite from the Tunceli region is the least known member of the IAESB (Çimen et al., 2014; Öztüfekçi-Önal et al., 2014).

Most papers on IAESB have been focused on the petrological characteristics of the volcanic rocks from the preserved ophiolitic sequences and mélanges. Moreover, the limited petrological studies on the mantle peridotites and chromite deposits in Anatolia (e.g., Uçurum et al., 2000; Uçurum and Koptagel, 2006; Uysal et al., 2012; 2015) do not include any data related to the Tunceli ophiolite. In other words, there is no published petrological data available on the chromite deposits in the Tunceli province where these ophiolitic units crop out. In this study, we present the first petrological data including whole-rock, mineral chemistry,

and PGE geochemistry of the chromitites and mantle peridotites within the Tunceli Ophiolite. We thus aim to provide the first insights on the petrology and geodynamic evolution of this ophiolite during the closure of the northern branch of the Neotethyan Ocean.

GEOLOGICAL FRAMEWORK

The tectonic setting of the Anatolia is characterized by the east-west trending IAESB that is located between the SCT and ATP. The SCT is thrust onto the IAESB that, in turn, occurs in tne north of the ATP (Göncüoğlu, 2010). The SCT and ATP are representative of two continental microplates, both detached at different times from the northern edge of the Gondwana plate. The IAESB bears fragments of the the northern branch of Neotethyan basin, i.e. the oceanic domain located between the SCT and ATP continental margins. The Tunceli ophiolite, cropping out in the areas of Ovacık, Pülümür and Mazgirt, is located in the eastern part of the IAESB (Fig. 1a, b).

According to the geology report of the study area by the MTA (Mineral Research and Exploration General Directorate) (2008), the ATP consists of Late Paleozoic metamorphic rocks (schists, marbles, meta-clastics, meta-basics) unconformably covered by the Middle Triassic to Cretaceous platform limestones. The IAESB is, in turn, represented by the Tunceli Ophiolite here consiting of the Late Cretaceous serpentinized mantle rocks. The relationships between the ATP and IAESB are sealed by the Eocene sedimentary and volcanics rocks topped by Oligo-Miocene volcanics with interlayered pyroclastic and lacustrine sediments (Fig. 1b). Whereas in the southern part of the study area the Tunceli Ophiolite directly overlains the ATP Paleozoic basement, in the north the Tunceli Ophiolite are thrust onto the Middle Triassic to Cretaceous platform limestones (Fig. 1b).

The Tunceli Ophiolite consists of serpentinized mantle peridotites, gabbros, sheeted dykes, pillow lavas and mudstones. The mantle peridotites mostly consist of harburzgites showing a transition to a level of dunites and chromitites. Some pyroxenite dykes were identified during the field survey. The mantle peridotites are completely serpentinized and intensively affected by brittle deformation leading to a pervasive cataclastic textures.

The chromitites are found as podiform-type in the highly serpentinized band located between harzburgites and dunites. The ore bodies are generally observed as irregular, isolated lenses and small batches. Most of them are massive and disseminated, whereas some minor bodies show a layered texture with nodular shape. The gangue of the deposits is essentially made up of serpentine minerals. The relict olivine crystals found at the center of the gangue minerals indicates that the ore deposits were originated inside the dunites. In spite of the intense serpentinization of the dunites, the chromitites are remarkably fractured but not affected by alteration.

ANALYTICAL METHODS

The ore and wall rock samples were collected from various locations within the chromite deposits (Fig. 1b). Representative ten ore and nine wall rock samples were selected for mineralogical and geochemical analyses. Major and trace elements of whole-rocks were analyzed by using an ICP-OES (ICP optical emission spectrometry) and ICP-MS (ICP mass spectrometry), respectively, at the Acme Analytical Laboratories (Canada). Total abundances of the major oxides and several minor elements were analysed by ICP-OES following a lithium metaborate/tetraborate fusion and dilute nitric digestion. Loss on ignition (LOI) was determined by weight difference after ignition at 1000°C. Some duplicated samples were analyzed in order to confirm the accuracy of the analyses. The concentrations of platinum group elements (PGE) were determined by using the nickel-sulfide fire assay pre-concentration followed by irradiation and analysis on the sulfide precipitate at the Maxxam Analytics International Corporation, Ontario, Canada. Detection limits were 10 ppb for Pt, Pd and Ru, 1 ppb for Rh and Os, 0.2 ppb for Ir, and 0.5 ppb for Au.

Mineral analyses by electron microprobe (EMP) were carried out on six ultramafic rock samples (harzburgite, dunite and pyroxenite) and seven chromitite samples. The samples affected by minor post-magmatic alteration were selected for analysis. However, some chromitites samples still have alteration evidence at grain boundaries and along fractures of the spinel group minerals. The PGMs, chromites and silicates were analyzed by electron microprobe using a Superprobe Jeol JXA 8200 at the Eugen F. Stumpfl Laboratory installed at the University of Leoben, Austria, using both ED and WD systems. Back scattered electron (BSE) images were obtained using the same instrument. During the analyses of chromites and silicates, the electron microprobe was operated in the WDS mode, with 15 kV of accelerating voltage and 10 nA of beam current. The analysis of Na, Mg, K, Al, Si, Ca, Ti, V, Cr, Zn, Mn, Fe and Ni were obtained using the Kα lines, and were calibrated on natural chromite, rhodhonite, ilmenite, albite, pentlandite, wollastonite, kaersutite, sphalerite and metallic vanadium. The following analyzing crystals were used: TAP for Na, Mg, Al, PETJ for K, Si, Ca and LIFH for Ti, V, Cr, Zn, Mn, Fe and Ni. The peak and backgrounds counting times were 20 and 10 seconds, respectively for the major elements. The PGMs were located by scanning polished sections under a reflected light microscope at 250-800 magnification. The PGMs with a size less than 5 microns were only qualitatively analyzed by EDS. The larger PGM swere quantitatively analyzed in the WDS mode, at 20 kV accelerating voltage and 10 nA beam current, and beam diameter of about 1 micron. The peak and backgrounds counting times were 15 and 5 seconds, respectively. The Kα lines were used for S, As, Fe and Ni; Lα for Ir, Ru, Rh, Pd and Pt, and Mα for Os. The reference materials were pure metals for the six PGE (Ru, Rh, Pd, Os, Ir, Pt), synthetic NiS, natural pyrite and niccolite for Ni, Fe S and As. The following diffracting crystals were selected: PETJ for S; PETH for Ru, Os, Rh; LIFH for Fe, Ni, Ir, Pt and TAP for As. Automatic corrections were performed for interferences involving Ru-Rh and Rh-Pd. 400 point analyses were carried out on spinel group minerals, 210 of which was from the chromitite samples while 190 points were from the host rock samples. Silicate minerals were analysed totally from 234 points, 40 of which were inclusions in spinels of chromitite and 194 main constituents of the peridotites. Moreover, the platinum group minerals (PGMs) were identified and analysed in two of the chromitite samples. The representative results of the EMP analysis for the minerals from both chromitite and tectonite samples are presented in Tables 1-4.

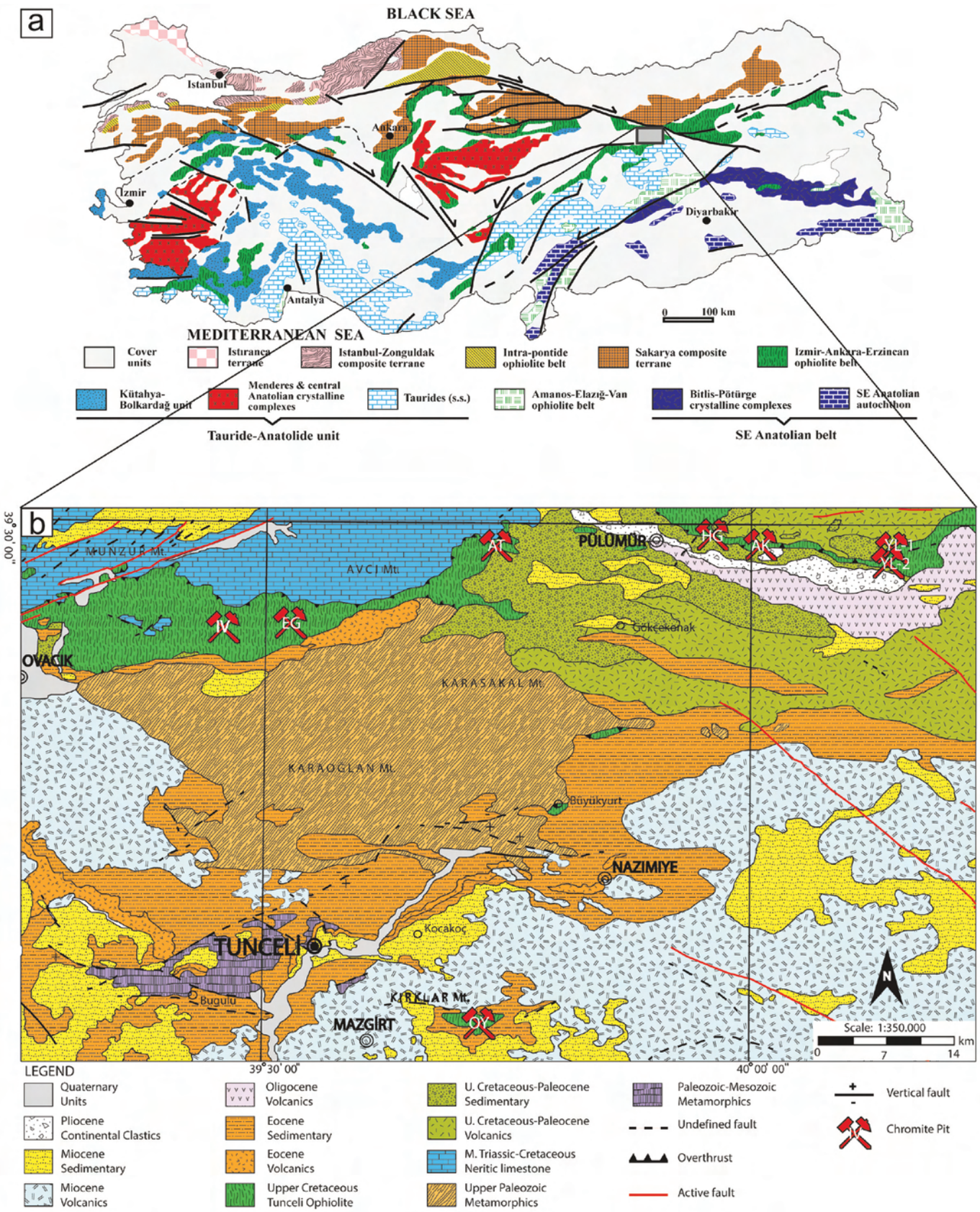

Fig. 1 - (a) Location of the study area in the tectonic sketch map of Anatolia (modified from Göncüolu, 2010), (b) Geological map of the study area (modified from MTA, 2008). IV=Ikvurak Mine, EG=Eskigedik Mine, AT=Atilla Mine, HG= Hasangazi Mine; AK=Aksu Mine; YL=Yldrm Mine; OY=Oymadal Mine.

Table 1 - Representative electron microprobe data for olivines from the peridotites.

Sample (wt%)	AT 1	AT 7	AT 12	AT 16	AT 20	AT 24	AT 28	AT 31	AT 39	AT 46	AT 58	AT 62	AT 64	AT 65	AT 68	AT 69	AT 70	AT 71	AT 72	IV 9	IV 10	IV 11
SiO_2	41	41.2	40.9	41.3	41.6	41.1	41.3	41.6	41.3	41	41.4	41.4	41.1	41	41.9	41.3	41.8	41.2	41.2	41.7	42.3	41.4
TiO_2	0.00	0.00	0.01	0.00	0.00	0.00	0.03	0.01	0.00	0.02	0.01	0.00	0.00	0.00	0.01	0.00	0.01	0.00	0.00	0.05	0.00	0.06
Al_2O_3	0.00	0.00	0.00	0.00	0.00	0.01	0.00	0.00	0.00	0.00	0.00	0.00	0.00	0.00	0.01	0.00	0.01	0.00	0.00	0.06	0.01	0.00
$FeO^{(t)}$	8.86	8.90	8.82	8.83	9.07	8.94	8.69	8.81	9.08	8.97	8.96	8.92	9.15	8.99	8.79	8.85	9.03	8.93	8.99	8.82	8.98	8.95
MnO	0.14	0.09	0.12	0.16	0.14	0.11	0.13	0.13	0.18	0.10	0.13	0.12	0.18	0.09	0.11	0.08	0.11	0.13	0.11	0.16	0.05	0.12
MgO	50.1	50.9	50	50.5	50.3	50.3	50.5	50.2	50.4	50.9	50.4	50	51	51.6	50.6	50.9	51.1	50.1	50.7	50.7	50.6	50.5
CaO	0.15	0.13	0.13	0.11	0.13	0.13	0.13	0.14	0.14	0.09	0.13	0.12	0.14	0.11	0.13	0.11	0.13	0.14	0.13	0.01	0.00	0.01
Na_2O	0.00	0.00	0.02	0.01	0.01	0.02	0.01	0.00	0.00	0.00	0.02	0.00	0.01	0.01	0.01	0.01	0.00	0.00	0.00	0.00	0.00	0.00
K_2O	0.02	0.00	0.00	0.02	0.00	0.00	0.00	0.00	0.00	0.01	0.00	0.00	0.00	0.01	0.00	0.01	0.00	0.00	0.00	0.00	0.00	0.00
Cr_2O_3	0.00	0.00	0.01	0.03	0.00	0.00	0.00	0.00	0.00	0.02	0.03	0.00	0.02	0.01	0.02	0.00	0.00	0.00	0.01	0.00	0.02	0.00
NiO	0.32	0.26	0.28	0.33	0.30	0.31	0.33	0.29	0.34	0.34	0.33	0.25	0.37	0.35	0.31	0.35	0.35	0.41	0.26	0.31	0.39	0.33
Total	100.6	101.5	100.3	101.3	101.5	100.9	101.1	101.2	101.4	101.5	101.4	100.9	102	102.2	101.9	101.6	102.5	100.8	101.4	101.8	102.3	101.4
Cation																						
Si	1.00	0.99	0.99	0.99	1.00	0.99	1.00	1.00	0.99	0.99	1.00	1.00	0.98	0.98	1.00	0.99	1.00	1.00	0.99	1.00	1.01	1.00
Ti	0.00	0.00	0.00	0.00	0.00	0.00	0.00	0.00	0.00	0.00	0.00	0.00	0.00	0.00	0.00	0.00	0.00	0.00	0.00	0.00	0.00	0.00
Al	0.00	0.00	0.00	0.00	0.00	0.00	0.00	0.00	0.00	0.00	0.00	0.00	0.00	0.00	0.00	0.00	0.00	0.00	0.00	0.00	0.00	0.00
$*Fe^{3+}$	0.02	0.03	0.02	0.02	0.00	0.02	0.01	0.00	0.02	0.04	0.01	0.00	0.05	0.08	0.00	0.03	0.01	0.01	0.03	0.00	0.00	0.00
$*Fe^{2+}$	0.18	0.18	0.18	0.17	0.18	0.18	0.17	0.18	0.18	0.18	0.18	0.18	0.18	0.18	0.17	0.18	0.18	0.18	0.18	0.17	0.18	0.18
Mn	0.00	0.00	0.00	0.00	0.00	0.00	0.00	0.00	0.00	0.00	0.00	0.00	0.00	0.00	0.00	0.00	0.00	0.00	0.00	0.00	0.00	0.00
Mg	1.81	1.82	1.81	1.81	1.8	1.81	1.81	1.81	1.81	1.82	1.81	1.81	1.82	1.83	1.81	1.82	1.81	1.81	1.82	1.81	1.8	1.81
Ca	0.00	0.00	0.00	0.00	0.00	0.00	0.00	0.00	0.00	0.00	0.00	0.00	0.00	0.00	0.00	0.00	0.00	0.00	0.00	0.00	0.00	0.00
Na	0.00	0.00	0.00	0.00	0.00	0.00	0.00	0.00	0.00	0.00	0.00	0.00	0.00	0.00	0.00	0.00	0.00	0.00	0.00	0.00	0.00	0.00
K	0.00	0.00	0.00	0.00	0.00	0.00	0.00	0.00	0.00	0.00	0.00	0.00	0.00	0.00	0.00	0.00	0.00	0.00	0.00	0.00	0.00	0.00
Cr	0.00	0.00	0.00	0.00	0.00	0.00	0.00	0.00	0.00	0.00	0.00	0.00	0.00	0.00	0.00	0.00	0.00	0.00	0.00	0.00	0.00	0.00
Ni	0.01	0.00	0.01	0.01	0.01	0.01	0.01	0.01	0.01	0.01	0.01	0.00	0.01	0.01	0.01	0.01	0.01	0.01	0.01	0.01	0.01	0.01
Sr	0.00	0.00	0.00	0.00	0.00	0.00	0.00	0.00	0.00	0.00	0.00	0.00	0.00	0.00	0.00	0.00	0.00	0.00	0.00	0.00	0.00	0.00
Total	3.01	3.03	3.01	3.01	3.00	3.02	3.01	3.00	3.01	3.04	3.01	3.00	3.05	3.07	3.00	3.03	3.01	3.01	3.03	3.00	3.00	3.00
Mg#	0.91	0.91	0.91	0.91	0.91	0.91	0.91	0.91	0.91	0.91	0.91	0.91	0.91	0.91	0.91	0.91	0.91	0.91	0.91	0.91	0.91	0.91

$*Fe^{2+}$ and Fe^{3+} are stoichiometrically calculated based on Droop's equation (1989).

Table 2 - Representative electron microprobe data for pyroxenes from the peridotites.

Sample	EG	EG	EG	EG	PR	PR	PR	PR	PR	AT	AT	AT	AT	IV	IV	IV	IV	IV	IV
	1	8	14	15	1	7	14	22	30	1	14	20	30	26	33	49	54	65	73
(wt%)	cpx1	cpx1	cpx2	cpx1	cpx1	cpx1	cpx1	cpx1	cpx1	cpx1	cpx2	cpx1	cpx2	opx	opx	opx	cpx1	cpx1	cpx2
SiO_2	54.8	54.9	54.1	54.6	54.9	54.4	53.4	53.5	54.5	52.9	53	54.3	53.2	57.6	57.5	57.9	53.8	53.4	53.2
TiO_2	0.05	0.00	0.13	0.01	0.04	0.01	0.03	0.00	0.02	0.00	0.11	0.03	0.07	0.00	0.07	0.05	0.00	0.03	0.11
Al_2O_3	0.84	0.73	1.61	0.85	1.37	1.29	1.26	1.18	1.34	1.56	2.68	0.90	1.90	1.59	1.45	1.56	1.45	1.81	2.82
$FeO^{(t)}$	2.05	1.76	2.78	2.20	1.86	1.92	2.02	1.67	2.17	2.13	3.11	2.10	2.87	5.87	5.89	5.85	1.96	2.27	3.37
MnO	0.07	0.07	0.08	0.04	0.09	0.07	0.10	0.07	0.07	0.03	0.16	0.09	0.10	0.13	0.17	0.17	0.09	0.11	0.10
MgO	18.2	18.2	17.7	17.9	18.2	18.0	18.1	18.1	18.2	17.6	16.1	18.2	16.9	35.2	34.3	34.3	18.0	17.7	16.5
CaO	23.8	24.4	23.9	23.4	23.8	24.3	23.8	24.5	23.7	23.6	23.9	23.5	23.9	1.10	0.80	1.30	24.1	23.5	23.7
Na_2O	0.07	0.10	0.13	0.10	0.04	0.02	0.06	0.03	0.04	0.07	0.19	0.12	0.16	0.01	0.00	0.00	0.09	0.07	0.24
K_2O	0.01	0.00	0.01	0.01	0.00	0.00	0.00	0.02	0.01	0.02	0.00	0.00	0.04	0.00	0.00	0.02	0.00	0.04	0.00
Cr_2O_3	0.51	0.44	0.31	0.46	0.44	0.58	0.52	0.55	0.54	0.71	0.94	0.50	0.44	0.50	0.47	0.62	0.64	0.82	1.08
NiO	0.05	0.11	0.00	0.08	0.07	0.00	0.10	0.05	0.03	0.06	0.08	0.06	0.00	0.07	0.06	0.04	0.02	0.08	0.03
Total	100.5	100.7	100.8	99.6	100.8	100.5	99.3	99.7	100.6	98.6	100.2	99.8	99.6	102	100.7	101.9	100.1	99.8	101.1
Cation																			
Si	1.98	1.98	1.97	1.98	1.97	1.96	1.95	1.94	1.96	1.92	1.93	1.95	1.94	1.94	1.97	1.96	1.95	1.94	1.94
$Al^{[4]}$	0.02	0.02	0.03	0.01	0.03	0.04	0.05	0.05	0.04	0.08	0.07	0.05	0.06	0.06	0.03	0.04	0.05	0.06	0.06
$Al^{[6]}$	0.01	0.01	0.01	0.02	0.03	0.02	0.00	0.00	0.02	0.04	0.05	0.02	0.02	0.01	0.03	0.03	0.01	0.02	0.01
Ti	0.00	0.00	0.00	0.00	0.00	0.00	0.00	0.00	0.00	0.00	0.00	0.00	0.00	0.00	0.00	0.00	0.00	0.00	0.00
$*Fe^{3+}$	0.00	0.01	0.01	0.00	0.00	0.01	0.04	0.05	0.00	0.02	0.00	0.02	0.03	0.04	0.00	0.00	0.03	0.02	0.03
$*Fe^{2+}$	0.06	0.04	0.05	0.07	0.06	0.05	0.02	0.00	0.06	0.08	0.09	0.06	0.06	0.13	0.17	0.17	0.03	0.05	0.04
Mn	0.00	0.00	0.00	0.00	0.00	0.00	0.00	0.00	0.00	0.00	0.00	0.00	0.00	0.00	0.00	0.00	0.00	0.00	0.00
Mg	0.98	0.98	0.98	0.97	0.98	0.97	0.98	0.98	0.98	0.89	0.88	0.95	0.92	1.77	1.75	1.74	0.97	0.96	0.97
Cr	0.01	0.01	0.01	0.01	0.01	0.02	0.02	0.02	0.02	0.03	0.03	0.01	0.01	0.01	0.01	0.02	0.02	0.02	0.02
Ni	0.00	0.00	0.00	0.00	0.00	0.00	0.00	0.00	0.00	0.00	0.00	0.00	0.00	0.00	0.00	0.00	0.00	0.00	0.00
Ca	0.92	0.94	0.92	0.91	0.92	0.94	0.93	0.95	0.91	0.92	0.93	0.92	0.94	0.04	0.03	0.05	0.93	0.91	0.93
Na	0.00	0.01	0.01	0.01	0.00	0.00	0.00	0.00	0.00	0.02	0.01	0.01	0.01	0.00	0.00	0.00	0.01	0.00	0.00
K	0.00	0.00	0.00	0.00	0.00	0.00	0.00	0.00	0.00	0.00	0.00	0.00	0.00	0.00	0.00	0.00	0.00	0.00	0.00
Sr	0.00	0.00	0.00	0.00	0.00	0.00	0.00	0.00	0.00	0.00	0.00	0.00	0.00	0.00	0.00	0.00	0.00	0.00	0.00
Total	4.00	4.00	4.00	4.00	4.00	4.00	4.00	4.00	4.00	4.00	4.00	4.00	4.00	4.00	4.00	4.00	4.00	4.00	4.00
Mg#	0.94	0.96	0.95	0.93	0.94	0.95	0.98	1.00	0.94	0.92	0.91	0.94	0.94	0.93	0.91	0.91	0.97	0.95	0.96

*Fe^{2+} and Fe^{3+} are stoichiometrically calculated based on Droop's equation (1989).

Table 3 - Representative electron microprobe data for chromian spinels from the peridotites.

Sample	AK	AK	AK	AK	AT	AT	AT	AT	EG	EG	EG	EG	IV	IV	IV	OY	OY	OY	PR	PR	PR
(wt%)	7	12	19	25	2	7	13	24	7	12	17	28	1	12	24	4	12	20	5	13	28
SiO_2	0.05	0.00	0.05	0.00	0.01	0.07	0.05	0.00	0.23	0.04	0.03	0.06	0.03	0.05	0.04	0.06	0.01	0.03	0.00	0.05	0.05
TiO_2	0.06	0.08	0.15	0.05	0.31	0.34	0.25	0.26	0.02	0.07	0.04	0.07	0.00	0.03	0.03	0.03	0.02	0.03	0.04	0.02	0.00
Al_2O_3	28.8	27.3	27.1	27.6	13.2	13.4	13.4	13.3	11.5	12.1	11.9	12.2	25.2	19.9	23.4	27.5	27.4	25.9	19.7	24.3	22.3
FeO	16.9	16.9	17.2	17.2	15.8	17.2	16.7	16.5	18.9	18.0	18.4	18.1	15.2	15.2	15.1	14.1	14.1	14.6	14.4	15.1	15.0
Fe_2O_3	10.6	10.5	9.77	9.84	8.98	9.12	8.96	9.30	5.35	6.06	5.60	5.36	4.27	4.29	4.07	7.13	7.81	7.15	4.50	4.09	3.91
MgO	12.6	12.3	12.5	12.2	11.8	10.7	11.2	11.4	9.5	10.2	9.9	10.1	13.3	13.1	13.4	14.4	13.9	13.8	13.4	13.2	13.0
MnO	0.29	0.36	0.30	0.32	0.38	0.40	0.38	0.33	0.43	0.38	0.35	0.40	0.30	0.34	0.32	0.24	0.27	0.34	0.29	0.27	0.30
Cr_2O_3	31.0	32.6	34.5	32.8	49.7	47.9	49.5	48.9	53.5	53.2	53.3	53.6	41.4	47.9	44.1	37.0	35.6	38.3	47.9	42.1	44.8
NiO	0.26	0.39	0.36	0.15	0.27	0.29	0.32	0.13	0.13	0.19	0.01	0.22	0.21	0.00	0.13	0.40	0.54	0.30	0.23	0.28	0.34
ZnO	0.00	0.00	0.00	0.00	0.00	0.00	0.00	0.00	0.00	0.00	0.00	0.00	0.00	0.00	0.00	0.00	0.00	0.00	0.00	0.00	0.00
V_2O_3	0.15	0.16	0.17	0.12	0.13	0.12	0.15	0.16	0.20	0.21	0.32	0.25	0.23	0.24	0.06	0.11	0.13	0.11	0.12	0.17	0.14
Total	100.6	100.5	102.1	100.4	100.5	99.6	100.9	100.3	99.7	100.4	99.9	100.3	100.2	101	100.6	100.9	99.9	100.5	100.5	99.5	99.9
Cation																					
Si	0.01	0.00	0.01	0.00	0.00	0.02	0.01	0.00	0.06	0.01	0.01	0.02	0.01	0.01	0.01	0.01	0.00	0.01	0.00	0.01	0.01
Ti	0.01	0.01	0.03	0.01	0.06	0.07	0.05	0.05	0.00	0.01	0.01	0.01	0.00	0.01	0.01	0.01	0.00	0.01	0.01	0.00	0.00
Al	8.14	7.79	7.63	7.88	4.00	4.14	4.06	4.06	3.58	3.73	3.71	3.75	7.22	5.79	6.72	7.72	7.78	7.36	5.76	7.03	6.50
Fe^{2+}	3.39	3.42	3.45	3.50	3.40	3.76	3.60	3.56	4.19	3.93	4.07	3.97	3.09	3.14	3.08	2.80	2.85	2.94	2.98	3.10	3.11
Fe^{3+}	1.91	1.91	1.76	1.80	1.74	1.79	1.74	1.81	1.07	1.19	1.11	1.06	0.78	0.80	0.75	1.28	1.41	1.30	0.84	0.76	0.73
Mg	4.52	4.45	4.46	4.42	4.53	4.17	4.31	4.39	3.76	3.97	3.88	3.94	4.82	4.81	4.85	5.10	5.00	4.95	4.93	4.81	4.78
Mn	0.06	0.07	0.06	0.06	0.08	0.09	0.08	0.07	0.10	0.08	0.08	0.09	0.06	0.07	0.07	0.05	0.05	0.07	0.06	0.06	0.06
Cr	5.88	6.24	6.52	6.29	10.1	9.88	10.1	10.0	11.2	11.0	11.1	11.1	7.95	9.35	8.49	6.96	6.78	7.3	9.37	8.17	8.73
Ni	0.05	0.08	0.07	0.03	0.06	0.06	0.07	0.03	0.03	0.04	0.00	0.05	0.04	0.00	0.02	0.08	0.10	0.06	0.05	0.06	0.07
Zn	0.00	0.00	0.00	0.00	0.00	0.00	0.00	0.00	0.00	0.00	0.00	0.00	0.00	0.00	0.00	0.00	0.00	0.00	0.00	0.00	0.00
V	0.01	0.02	0.02	0.01	0.01	0.01	0.02	0.02	0.02	0.02	0.03	0.03	0.02	0.02	0.01	0.01	0.01	0.01	0.01	0.02	0.01
Total	24.0	24.0	24.0	24.0	24.0	24.0	24.0	24.0	23.9	24.0	24.0	24.0	24.0	24.0	24.0	24.0	24.0	24.0	24.0	24.0	24.0
Cr#	0.42	0.44	0.46	0.44	0.72	0.70	0.71	0.71	0.76	0.75	0.75	0.75	0.52	0.62	0.56	0.47	0.47	0.50	0.62	0.54	0.57
Mg#	0.57	0.57	0.56	0.56	0.57	0.53	0.54	0.55	0.47	0.50	0.49	0.50	0.61	0.61	0.61	0.65	0.64	0.63	0.62	0.61	0.61

*Fe^{2+} and Fe^{3+} are stoichiometrically calculated based on Droop's equation (1989).

Table 4 - Representative electron microprobe data for chromian spinels from the chromitites.

Sample (wt%)	AK 7	AK 16	AK 30	AT 5	AT 22	AT 30	EG 3	EG 9	EG 11	HG 3	HG 9	HG 10	IV 2	IV 4	IV 12	OY 1	OY 7	OY 27	YL 2	YL 6	YL 27
SiO_2	0.06	0.00	0.00	0.00	0.01	0.00	0.00	0.02	0.03	0.00	0.00	0.00	0.05	0.02	0.06	0.00	0.04	0.02	0.08	0.00	0.03
TiO_2	0.22	0.14	0.19	0.12	0.13	0.20	0.12	0.11	0.04	0.20	0.18	0.10	0.04	0.07	0.18	0.15	0.18	0.21	0.13	0.10	0.11
Al_2O_3	15.6	15.9	16.0	18.5	18.6	18.2	8.18	8.35	8.21	18.2	18.5	17.2	5.61	5.74	5.68	13.2	13.2	12.4	8.52	8.5	8.46
FeO	14.5	13.8	13.9	14.0	13.8	13.5	14.4	14.7	14.0	13.7	13.9	14.3	14.2	14.3	14.3	18.1	19.1	19.7	15.1	14.8	15.7
Fe_2O_3	3.99	4.59	4.34	4.03	3.80	3.94	4.18	3.68	4.54	4.51	4.37	4.18	2.35	2.03	2.11	4.16	3.21	2.62	2.95	2.90	2.69
MgO	12.7	13.1	12.9	13.2	13.3	13.3	12.3	12.2	12.4	13.6	13.3	12.8	12.0	12.0	12.0	10.1	9.60	8.93	11.8	11.8	11.4
MnO	0.25	0.31	0.28	0.22	0.27	0.28	0.26	0.29	0.33	0.27	0.32	0.28	0.30	0.34	0.25	0.37	0.24	0.36	0.36	0.39	0.33
Cr_2O_3	51.5	51.3	50.9	48.6	48.9	49.0	60.8	61.3	60.6	49.2	48.4	50.0	65.3	65.3	65.0	53.1	53.4	54.3	61.5	61.2	61.5
NiO	0.32	0.44	0.46	0.43	0.62	0.54	0.03	0.03	0.14	0.46	0.43	0.38	0.14	0.11	0.25	0.10	0.10	0.18	0.36	0.20	0.16
ZnO	0.00	0.00	0.00	0.00	0.00	0.00	0.00	0.00	0.00	0.00	0.00	0.00	0.00	0.00	0.00	0.00	0.00	0.00	0.00	0.00	0.00
V_2O_3	0.13	0.09	0.09	0.09	0.13	0.06	0.13	0.07	0.07	0.10	0.13	0.03	0.03	0.06	0.03	0.19	0.22	0.21	0.03	0.06	0.03
Total	99.3	99.6	99.1	99.2	99.6	99.1	100.4	100.7	100.4	100.2	99.5	99.2	100.1	99.9	99.8	99.5	99.3	99.0	100.8	100.0	100.4
Cation																					
Si	0.01	0.00	0.00	0.00	0.00	0.00	0.00	0.00	0.01	0.00	0.00	0.00	0.01	0.01	0.01	0.00	0.01	0.00	0.02	0.00	0.01
Ti	0.04	0.03	0.04	0.02	0.02	0.04	0.02	0.02	0.01	0.04	0.03	0.02	0.01	0.01	0.04	0.03	0.04	0.04	0.03	0.02	0.02
Al	4.70	4.77	4.81	5.50	5.51	5.40	2.53	2.57	2.53	5.36	5.49	5.14	1.76	1.80	1.78	4.09	4.11	3.91	2.62	2.64	2.62
Fe^{2+}	3.10	2.93	2.96	2.94	2.89	2.86	3.14	3.22	3.07	2.85	2.91	3.04	3.17	3.18	3.18	3.97	4.21	4.39	3.29	3.26	3.45
Fe^{3+}	0.77	0.88	0.83	0.76	0.72	0.75	0.82	0.72	0.89	0.85	0.82	0.80	0.47	0.41	0.42	0.82	0.64	0.53	0.58	0.57	0.53
Mg	4.84	4.94	4.92	4.95	4.96	5.01	4.82	4.74	4.84	5.04	4.97	4.85	4.75	4.74	4.76	3.96	3.77	3.54	4.59	4.63	4.47
Mn	0.05	0.07	0.06	0.05	0.06	0.06	0.06	0.06	0.07	0.06	0.07	0.06	0.07	0.08	0.06	0.08	0.05	0.08	0.08	0.09	0.07
Cr	10.4	10.3	10.3	9.70	9.70	9.80	12.6	12.6	12.5	9.70	9.60	10.0	13.7	13.7	13.7	11.0	11.1	11.4	12.7	12.7	12.8
Ni	0.07	0.09	0.10	0.09	0.12	0.11	0.01	0.01	0.03	0.09	0.09	0.08	0.03	0.02	0.05	0.02	0.02	0.04	0.08	0.04	0.03
Zn	0.00	0.00	0.00	0.00	0.00	0.00	0.00	0.00	0.00	0.00	0.00	0.00	0.00	0.00	0.00	0.00	0.00	0.00	0.00	0.00	0.00
V	0.01	0.01	0.01	0.01	0.01	0.01	0.01	0.01	0.01	0.01	0.01	0.00	0.00	0.01	0.00	0.02	0.02	0.02	0.00	0.01	0.00
Total	24.0	24.0	24.0	24.0	24.0	24.0	24.0	24.0	24.0	24.0	24.0	24.0	24.0	24.0	24.0	24.0	24.0	24.0	24.0	24.0	24.0
Cr#	0.77	0.78	0.78	0.77	0.77	0.77	0.80	0.80	0.80	0.77	0.77	0.77	0.81	0.81	0.81	0.73	0.73	0.72	0.79	0.80	0.79
Mg#	0.61	0.63	0.62	0.63	0.63	0.64	0.61	0.60	0.61	0.64	0.63	0.61	0.60	0.60	0.60	0.50	0.47	0.45	0.58	0.59	0.56

*Fe^{2+} and Fe^{3+} are stoichiometrically calculated based on Droop's equation (1989).

RESULTS

Petrography

21 representative chromitite and 19 ultramafic wall-rock samples, collected from various mining sites, were examined under polarized and ore microscope to determine mineral abundances and textural characteristics. The ultramafics were composed of variable proportions of olivine, clinopyroxene and orthopyroxene with accessory of amount of spinel. Modal mineralogy and textural features indicate that the wall rocks are harzburgitic and dunitic mantle tectonites. Fresh host rocks are rare. In the altered samples talc and tremolite may occur in addition to serpentine. The spinel group minerals of these samples are the least affected by secondary processes.

Comparatively fresh samples of the peridotites are restricted to the mines from the Hasangazi and Atilla areas. The peridotites are mostly harzburgites with low but variable abundance of clinopyroxene. The widespread serpentinization mostly erased the primary textural features but mosaic, granoblastic textures are locally preserved. Some of the harzburgite samples have relatively high amounts of fine-grained, interstitial clinopyroxene whose formation may be the result of melt-rock interaction. Although primary olivine is mostly replaced by serpentine, relict crystals were observed through the mesh-textured serpentine (Fig. 2a). The orthopyroxenes were commonly replaced by bastite. Fine- to medium- grained (up to 1 mm) crystals of spinel group minerals occur as inclusions in the main minerals or disseminated in the rocks (Fig. 2a, b). Disseminated spinels in the harzburgites generally occur as euhedral or elongated crystals. They are generally fractured due to volume change during serpentinization. The fractures are mostly filled by serpentine aggregates and, sometimes, by talc and tremolite.

Dunite samples are made up of > 90% olivine, orthopyroxene < 3%, clinopyroxene < 4% and spinel < 3%. Black spinel crystals in accessory amount are subhedral. The samples are largely serpentinized. In certain instances, the samples do not have any primary minerals due to pervasive serpentinization that can reach up to 95% of the total surface area. Talc and tremolite occur in addition to serpentine minerals. Serpentine and talc even fill out the fractures of the spinel crystals that are disseminated in the samples (Fig. 2c). Original textural features of the serpentinized dunites, i.e., porphyroclastic texture, were almost completely replaced by mesh texture.

The chromitites in the study area are mainly represented by small bodies with massive, disseminated, banded or nodular forms. Banded chromite ore bodies display schlieren texture, characterized by parallel layers of massive to semi-massive chromitite alternating with serpentinized dunite. Chromian spinel crystals, variable in size from fine- to coarse-grained (0.2-3.1 mm), are euhedral to anhedral. Most of the chromian spinel crystals are highly fractured due to cataclastic deformation (Fig. 2d). Along fractures and at rims, the crystals are darker compared to inner fresh cores. During alteration ferrian chromite and magnetite were formed as a consequence of Cr loss. Chromite crystals, especially in disseminated and layered forms of chromitites, occur in the interstitial matrix of serpentine accompained by occasional amont of talc and chlorite replacing primary olivine and orthopyroxene. Moreover, fractures of the crystals are filled out by serpentine and talc. In spinel crystals, silicate mineral inclusions (e.g., olivine) may be observed. In addition, PGM, awaurite and orcelite were identified in chromian spinels of the chromitites (Fig. 2e). Surprisingly, a small grain of platinum (about 1 μm in size) was found in a grain of pentlandite, occurring in the serpentinized peridotite hosting the chromitite (Fig. 2f).

Mineralogy and Mineral Chemistry

Mantle peridotites

Olivine is the most abundant phase in the tectonites of the Tunceli Ophiolite and representative compositions are reported in Table 1. The analyses display very slight compositional differences in Fo values of dunite and hazburgite that range between 90.7-91.5 and 91.0-91.2 mol%, respectively. Additionally, NiO contents of olivines from dunite and harzburgite are low, varying between 0.24-0.41 and 0.31-0.39 wt%, respectively. The MnO contents of olivine in both rock types are between 0.05 and 0.21 wt%, and the CaO content is very low, less than 0.15 wt% for all samples (Table 1).

In most samples, diopsidic clinopyroxene ($Wo_{44.1-48.9}En_{45.9-52.5}Fs_{2.6-5.5}$) is the only preserved pyroxene, while the occurrence of relict enstatitic orthopyroxene ($Wo_{0.9-10.3}En_{82.4-90.4}Fs_{7.3-11.0}$) is restricted to few harzburgite samples. $Mg/(Mg+Fe^{2+})$ of clinopyroxene are between 0.90-1.00 while those of orthopyroxene vary in a narrow range of 0.91-0.95. The Al_2O_3 content of clinopyroxene ranges between 0.7 and 3.0 wt%, whereas orthopyroxene display a narrow variation from 1.4 to 1.8 (wt%). There is no compositional difference in clinopyroxene controlled by the presence of orthopyroxene. The TiO_2 and Na_2O contents of clinopyroxene are < 0.27 wt% and < 0.29 wt%, respectively, whereas lower values (TiO_2 < 0.10 wt% and Na_2O < 0.03 wt%) were measured for orthopyroxene. Both pyroxenes display overlapping compositional ranges in Cr_2O_3 (0.16-1.34 wt%). The secondary clinopyroxenes, reflecting rock-melt interaction, are well distinct for higher $FeO^{(t)}$, TiO_2 and Al_2O_3 contents than the primary clinopyroxenes (Fig. 3).

The chromian spinels of the peridotites vary in compositions from spinel (OY and AK mines) and magnesiochromite (IV and AT mines) to chromite (EG mine) (Table 3; Fig. 4). In other terms, the spinel and magnesiochromite compositions with lower Cr# (39-63) and higher Mg# (52-65) values are related to harzburgite while chromite composition with higher Cr# (68-77) and lower Mg# (43-57) are associated with dunite. The most Cr-rich spinels in the harzburgites contains low TiO_2 concentrations (< 0.1 wt%), whereas chromites in the dunite samples from the EG mine have relatively higher TiO_2 concentrations up to 0.41 wt%. Mg# > 0.40 of the chromian spinels suggest that the mineral was not chemically affected by alteration (not shown).

Chromitites

The chromitites within the Tunceli Ophiolite are composed of 47.7-66.6 wt% of Cr_2O_3, 4.60-19.1 wt% of Al_2O_3, 1.3-6.2 wt% of Fe_2O_3, ≤ 0.27 wt% of TiO_2 (Table 4). Their Cr# (0.63-0.89) and Mg# values (0.44-0.66) indicate magnesiochromite composition for all the chromian spinels of chromitites except for those from the OY mine (Fig. 4). The chromian spinels from the OY mine have the lowest Mg# values corresponding to chromite composition. The magnesiochromite crystals from the IV chromitites show the lowest Al_2O_3, TiO_2 and Fe_2O_3 (wt%) concentrations (Table 4).

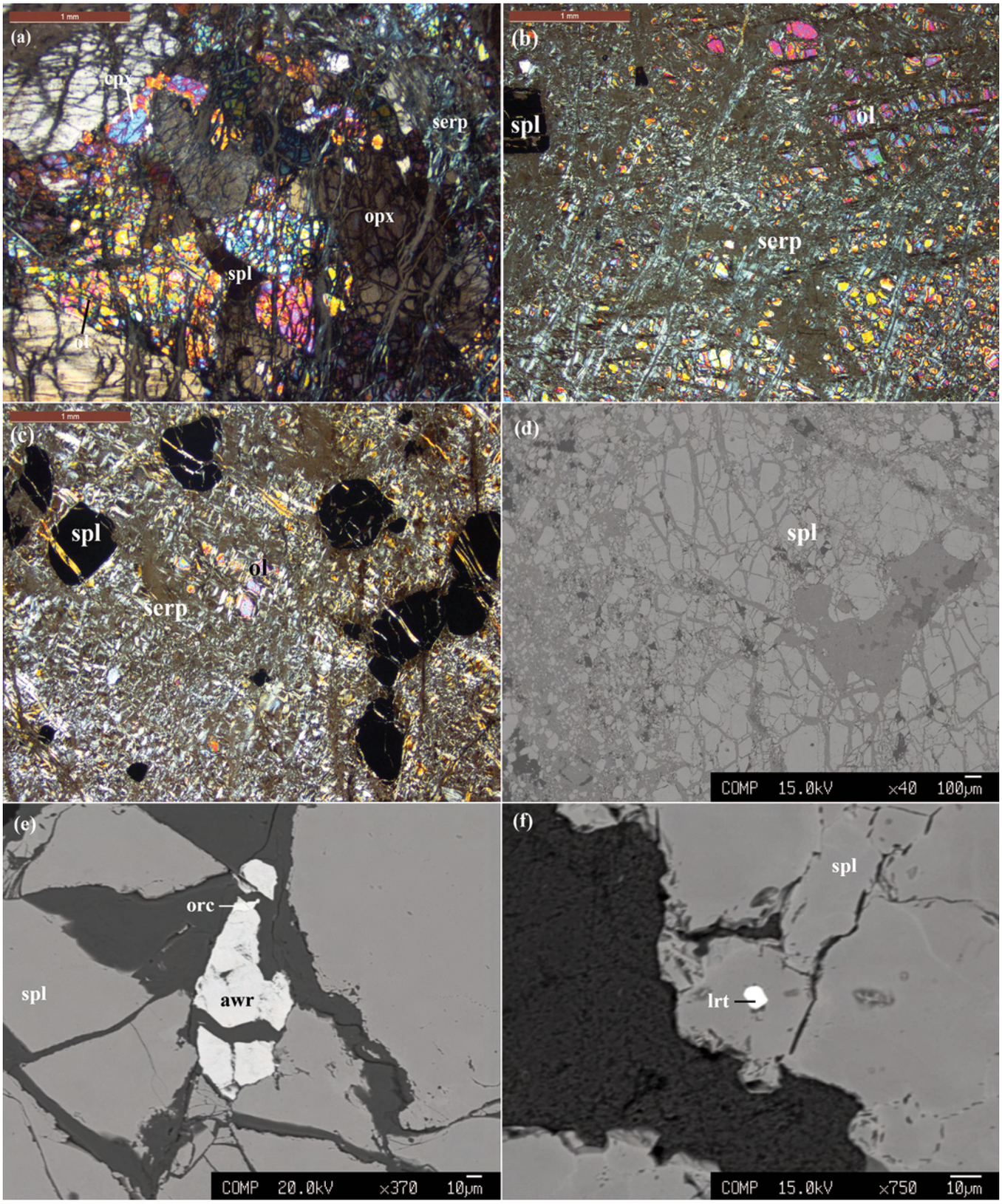

Fig. 2 - Microphotographs showing, (a) microstructure of a relatively preserved harzburgite, (b) serpentinized harburgite with relicts of the primary phases, (c) serpentinized dunite with disseminated spinel crystals. Back-scattered electron images of, (d) highly fractured and brecciated chromitite. (e) awaruite (Ni-Fe alloy) and orcelite (Ni arsenide) in chromitite samples. (f) laurite (RuS_2) in chromian spinel crystals (ol- olivine, cpx- clinopyroxene, opx- orthopyroxene, serp- serpentine, spl- spinel, awr- awaruite, orc- orcelite, lrt- laurite).

High Mg# (> 0.40) (Sobolev and Logvinova, 2005) and low $Fe^{3+}/(Fe^{3+}+Al+Cr)$ values for the chromian spinels indicate that they are unaffected by alteration. The silicate inclusions in the chromitite samples comprise olivine (Fo = 96.5-97.2), diopsidic clinopyroxene ($Wo_{45.6-48.1}En_{49.0-51.1}Fs_{2.8-3.4}$), pargasitic amphibole and phlogopite.

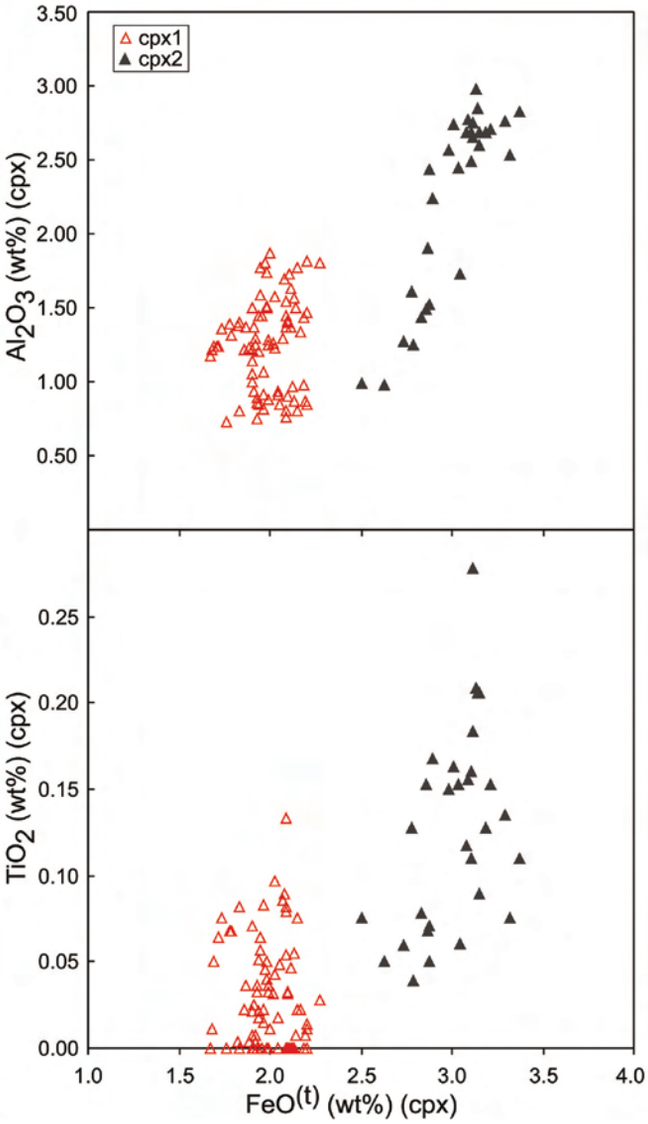

Fig. 3 - Variation of Al_2O_3 and TiO_2 (wt%) contents of clinopyroxene againts $FeO^{(t)}$ displaying compositional difference of primary and secondary clinopyroxenes in the harzburgite samples.

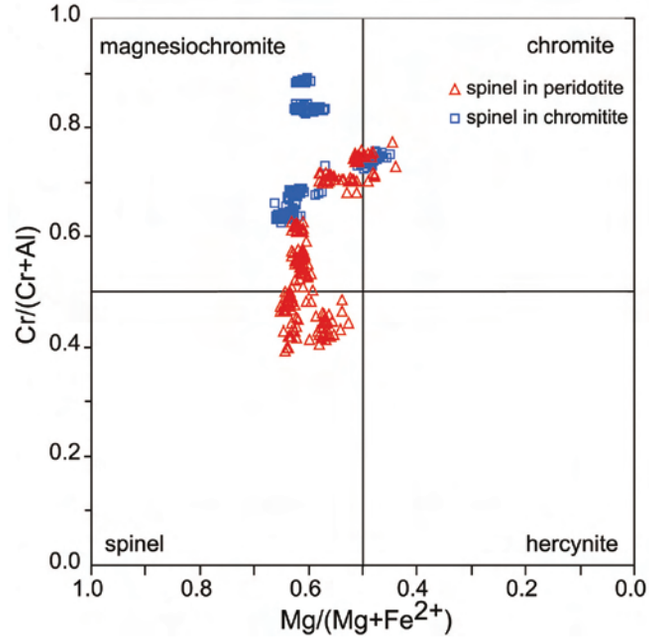

Fig. 4 - Classification and compositional variation of chromian spinel from peridotites and chromitites in terms of Cr/(Cr + Al) and Mg/(Mg + Fe^{2+}).

Whole rock geochemistry

Highly variable loss on ignition (LOI) values were observed for the mantle peridotites (2.5 16.6 wt%; Table 5). These values are related to variable extent of hydrothermal alteration detected during petrographic observations. Whole-rock compositions were therefore corrected on a volatile-free basis for the mantle peridotites. However, the LOI values of chromitite samples are between 0.1-2.0 wt% which reflect scarce influence of secondary processes. Moreover, the trace elements immobile during hydrothermal alteration processes (e.g., V, Co, Sc, Ga and Ni, Pearce and Cann, 1973; Floyd and Winchester, 1978), were used to minimize the effect of this alteration. Analytically, the rare earth element concentrations are mostly below the detection limits (Table 5).

Mantle peridotites

Major and trace element concentrations of the mantle peridotites are given in Table 5. MgO contents vary from 32.35 to 42.86 wt%, showing variable depletion relative to the primitive mantle (PM; 38.8 wt%, McDonough and Sun, 1995). The concentrations of other major oxides (wt%) such as SiO_2, Al_2O_3, CaO and Fe_2O_3 range between 39.43-47.38; 0.12-3.86; 0.12-2.99 and 7.37-11.08, respectively. CaO and Al_2O_3 contents are also depleted relative to PM (CaO = 3.5 wt%; Al_2O_3 = 4.4 wt%; McDonough and Sun, 1995).

The MgO/SiO_2 vs Al_2O_3/SiO_2 diagram (Fig. 5) can be used in order to point out possible Mg loss in abyssal peridotites (Snow and Dick, 1995). Niu (2004) suggests that, the 'terrestrial array' represents a magmatic depletion trend from a primitive mantle (MgO/SiO_2 ~ 0.85; Al_2O_3/SiO_2 ~ 0.1) to highly depleted harzburgitic composition (MgO/SiO_2 ~ 1.1 and Al_2O_3/SiO_2 ~ 0). The MgO/SiO_2 vs Al_2O_3/SiO_2 ratios of the mantle peridotites of this study vary between 0.82-1.28 and 0.002-0.086, respectively. Most of the samples plot below the mantle array. On the other hand, two dunite samples (from IV and AT mines) plot above the mantle array. While the AT mine has highest MgO/SiO_2 (1.28) and lowest Al_2O_3/SiO_2 (0.002) ratios, the OY mine has lowest MgO/SiO_2 (0.82) and highest Al_2O_3/SiO_2 (0.086) ratios relative to the other mantle peridotites (Fig. 5).

The variations of SiO_2, Al_2O_3, CaO, Fe_2O_3, Sc, Ga, V, Ni againts MgO (Fig. 6) were used to understand the possible tectonic environment of the peridotites (Niu et al., 1997; Parkinson and Pearce, 1998, Uysal et al., 2012). While the samples from EG, HG, AK, YL mines mostly plot in or close to the abyssal peridotite field, the samples from AT and IV mines (dunites) plot in or close the Supra-Subduction Zone (SSZ) field. Overall, higher SiO_2, Al_2O_3, CaO, Fe_2O_3, Sc, Ga, V, Ni associated with lower MgO concentrations are consistent with an abyssal affinity (Fig. 6).

Chromitites

Major and trace element concentrations of the chromitites are presented in Table 5. The Cr_2O_3 contents (12.29-17.35 wt%) are lower than those observed for other chromite deposits in Turkey (Günay and Çolakoğlu, 2011). The samples

Table 5 - Whole rock major and trace element data of the peridotites and chromitites.

Rock Type	*Chromitites*										*Peridotites*								
Sample	**EG-C1**	**EG-C1**	**EG-C3**	**AK-C1**	**HG-C1**	**AT-C1**	**IV-C1**	**YL-C1**	**YL-C2**	**OY-C1**	**EG-Y1**	**AK-Y1**	**HG-Y1**	**AT-Y1**	**IV-Y1**	**YL-Y1**	**YL-Y2**	**YL-Y3**	**OY-Y1**
SiO_2 (wt %)	1.88	1.05	1.19	2.57	3.31	15.47	5.65	5.03	6.05	2.58	37.69	39.41	42.50	33.28	33.37	39.68	40.89	40.81	40.39
Al_2O_3	6.51	21.02	22.31	15.53	17.26	10.80	4.06	7.30	13.66	17.52	0.12	3.42	0.87	0.12	0.10	0.62	0.33	0.57	0.38
Fe_2O_3	12.31	13.30	11.63	11.44	10.36	9.98	10.45	12.90	12.36	13.17	7.20	9.81	7.80	7.96	6.15	7.53	7.22	7.62	7.33
MgO	12.07	15.36	15.52	15.54	15.92	25.97	16.37	17.40	16.67	15.35	37.55	32.35	36.63	41.94	42.86	38.66	35.14	36.58	34.61
CaO	0.16	0.04	<0.01	<0.01	1.92	0.02	<0.01	<0.01	0.67	1.03	0.12	2.65	1.08	0.22	0.10	0.79	0.14	0.50	0.03
Na_2O	<0.01	<0.01	<0.01	<0.01	<0.01	<0.01	<0.01	<0.01	<0.01	<0.01	<0.01	0.01	<0.01	0.01	0.05	0.01	<0.01	<0.01	<0.01
K_2O	<0.01	<0.01	<0.01	<0.01	<0.01	<0.01	<0.01	<0.01	0.01	<0.01	<0.01	<0.01	<0.01	<0.01	<0.01	0.01	<0.01	<0.01	<0.01
TiO_2	<0.01	0.11	0.09	0.04	0.02	0.08	<0.01	<0.01	0.13	0.09	<0.01	0.02	<0.01	<0.01	<0.01	<0.01	<0.01	<0.01	<0.01
P_2O_5	<0.01	<0.01	<0.01	<0.01	<0.01	<0.01	<0.01	<0.01	<0.01	<0.01	0.01	0.01	<0.01	<0.01	<0.01	<0.01	<0.01	<0.01	<0.01
MnO	0.12	0.12	0.11	0.14	0.12	0.10	0.11	0.13	0.13	0.16	0.10	0.15	0.11	0.11	0.08	0.11	0.09	0.12	0.10
Cr_2O_3	15.77	16.66	16.19	14.97	14.61	12.29	15.49	15.91	15.40	17.36	0.28	0.48	0.37	0.38	0.44	0.40	0.35	0.41	0.35
LOI	1.00	0.10	0.20	2.40	3.90	7.50	2.10	2.10	2.50	2.00	16.60	11.50	10.30	15.60	16.50	11.90	15.00	13.10	16.00
Sum	49.89	67.88	67.38	62.77	67.49	82.41	54.32	60.86	67.66	69.31	99.96	99.94	99.95	99.94	99.92	99.92	99.40	99.95	99.42
Ni (ppm)	654	1173	1207	960	965	1647	1024	1116	979	1072	2044	1269	2045	2207	2481	1943	1942	1982	1990
Sc	7.00	5.00	5.00	7.00	7.00	6.00	5.00	7.00	10.00	5.00	5.00	15.00	10.00	4.00	3.00	10.00	8.00	10.00	7.00
Ba	<1	22.00	8.00	<1	2.00	<1	<1	<1	9.00	9.00	<1	3.00	<1	<1	<1	<1	4.00	<1	5.00
Co	113	113	100	120	105	98	122	121	106	116	110	119	110	102	88	89	106	105	102
Cs	<0.1	<0.1	0.20	<0.1	<0.1	<0.1	<0.1	<0.1	0.20	0.20	<0.1	<0.1	<0.1	<0.1	<0.1	0.40	<0.1	0.50	<0.1
Ga	11.7	26.8	28.4	20.2	19.1	13.9	6.2	11.0	18.7	22.7	0.80	2.40	1.20	<0.5	<0.5	0.80	<0.5	1.10	<0.5
Hf	0.10	<0.1	<0.1	<0.1	<0.1	0.10	<0.1	<0.1	<0.1	<0.1	<0.1	<0.1	<0.1	0.10	<0.1	0.20	<0.1	<0.1	<0.1
Nb	<0.1	0.60	3.80	<0.1	<0.1	0.20	<0.1	<0.1	1.00	0.90	<0.1	<0.1	<0.1	0.10	<0.1	<0.1	0.30	<0.1	0.90
Rb	0.60	4.00	5.10	0.80	0.70	0.60	0.90	1.00	2.70	3.70	<0.1	<0.1	<0.1	<0.1	<0.1	0.50	0.70	0.90	0.40
Sr	5.50	3.00	1.90	<0.5	52.90	<0.5	<0.5	<0.5	3.10	18.60	3.10	2.30	3.40	1.80	0.80	3.00	2.60	4.50	3.10
Th	<0.2	<0.2	<0.2	<0.2	<0.2	<0.2	<0.2	<0.2	0.20	<0.2	<0.2	<0.2	<0.2	<0.2	<0.2	<0.2	<0.2	<0.2	<0.2
U	<0.1	0.20	0.20	<0.1	<0.1	<0.1	<0.1	<0.1	0.30	0.10	<0.1	<0.1	<0.1	<0.1	<0.1	<0.1	<0.1	<0.1	<0.1
V	578	693	635	715	746	443	406	524	554	751	20	63	61	20	20	44	39	51	29
W	0.7	<0.5	<0.5	<0.5	0.5	<0.5	<0.5	<0.5	0.5	<0.5	<0.5	<0.5	<0.5	<0.5	0.5	<0.5	<0.5	<0.5	0.7
Zr	1.20	1.10	1.20	0.20	<0.1	0.20	0.90	0.10	1.50	0.90	<0.1	0.20	<0.1	<0.1	0.70	1.80	0.50	<0.1	0.80
Y	<0.1	0.20	<0.1	<0.1	0.10	<0.1	<0.1	<0.1	0.70	<0.1	<0.1	0.70	<0.1	<0.1	<0.1	<0.1	0.20	<0.1	0.10
La	0.40	0.70	0.50	<0.1	<0.1	0.30	<0.1	<0.1	0.70	0.50	<0.1	<0.1	0.10	<0.1	0.30	<0.1	1.00	<0.1	1.00
Ce	<0.1	0.30	0.40	<0.1	<0.1	<0.1	<0.1	<0.1	0.50	0.30	<0.1	<0.1	<0.1	<0.1	<0.1	<0.1	0.30	<0.1	0.50
Pr	0.09	0.05	0.04	0.07	0.06	0.08	0.06	0.06	0.07	0.06	<0.02	<0.02	<0.02	0.09	0.07	0.06	<0.02	<0.02	0.05
Nd	<0.3	<0.3	<0.3	<0.3	<0.3	<0.3	<0.3	<0.3	0.30	<0.3	<0.3	<0.3	<0.3	<0.3	<0.3	<0.3	<0.3	<0.3	<0.3
Sm	<0.05	0.12	0.14	<0.05	<0.05	0.05	0.09	0.08	0.21	0.17	<0.05	<0.05	<0.05	0.13	0.07	0.13	<0.05	<0.05	<0.05
Eu	<0.02	<0.02	0.03	<0.02	<0.02	<0.02	<0.02	<0.02	<0.02	<0.02	<0.02	0.02	<0.02	<0.02	<0.02	<0.02	<0.02	<0.02	<0.02
Gd	0.07	<0.05	<0.05	<0.05	0.10	<0.05	<0.05	<0.05	0.07	0.05	<0.05	0.07	<0.05	0.07	0.14	0.06	<0.05	<0.05	<0.05
Tb	<0.01	0.02	<0.01	<0.01	<0.01	<0.01	<0.01	<0.01	0.01	<0.01	<0.01	0.01	<0.01	<0.01	<0.01	<0.01	<0.01	<0.01	<0.01
Dy	<0.05	<0.05	<0.05	0.08	0.07	<0.05	<0.05	<0.05	0.08	<0.05	<0.05	0.09	<0.05	<0.05	0.06	<0.05	<0.05	<0.05	<0.05
Ho	<0.02	<0.02	<0.02	<0.02	<0.02	<0.02	<0.02	<0.02	<0.02	<0.02	<0.02	<0.02	<0.02	<0.02	<0.02	<0.02	<0.02	<0.02	<0.02
Er	<0.03	0.05	<0.03	<0.03	<0.03	<0.03	<0.03	0.05	0.04	<0.03	<0.03	0.07	<0.03	<0.03	<0.03	0.05	<0.03	<0.03	<0.03
Tm	<0.01	<0.01	<0.01	<0.01	<0.01	<0.01	<0.01	<0.01	0.01	<0.01	<0.01	<0.01	<0.01	<0.01	<0.01	<0.01	<0.01	<0.01	<0.01
Yb	<0.05	<0.05	<0.05	<0.05	<0.05	<0.05	<0.05	<0.05	0.07	<0.05	<0.05	<0.05	<0.05	<0.05	<0.05	<0.05	<0.05	<0.05	<0.05
Lu	<0.01	<0.01	0.01	<0.01	<0.01	<0.01	<0.01	<0.01	0.02	0.01	<0.01	<0.01	<0.01	<0.01	<0.01	<0.01	<0.01	<0.01	<0.01
Mo	3.10	0.30	<0.1	1.90	1.70	2.80	2.50	2.10	<0.1	<0.1	<0.1	0.20	0.40	0.20	<0.1	0.30	<0.1	0.10	<0.1
Cu	3.60	3.10	2.20	7.70	2.40	3.90	5.80	3.00	0.90	1.20	2.60	38.8	3.70	3.20	1.10	16.0	16.7	13.8	18.7
Zn	1.00	1.00	<1	6.00	<1	2.00	4.00	<1	3.00	1.00	30	23	22	32	22	27	34	28	24
Au	0.70	<0.5	<0.5	<0.5	<0.5	<0.5	<0.5	<0.5	0.60	1.10	1.10	2.70	1.40	1.30	<0.5	1.60	3.00	<0.5	1.60

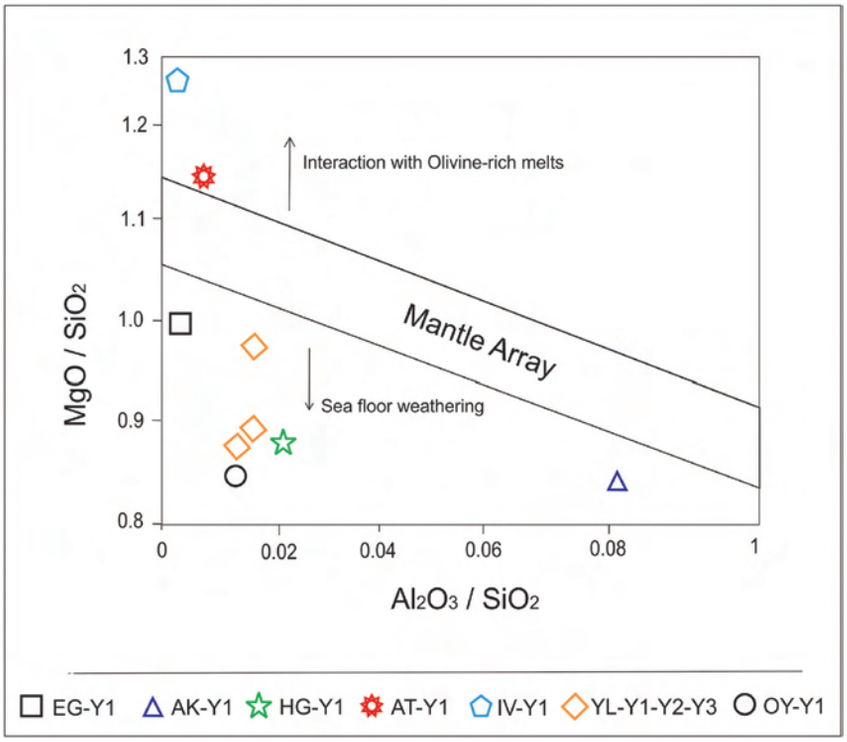

Fig. 5 - MgO/SiO_2 vs Al_2O_3/SiO_2 diagram for the mantle peridotites (modified from Uysal et al., 2012).

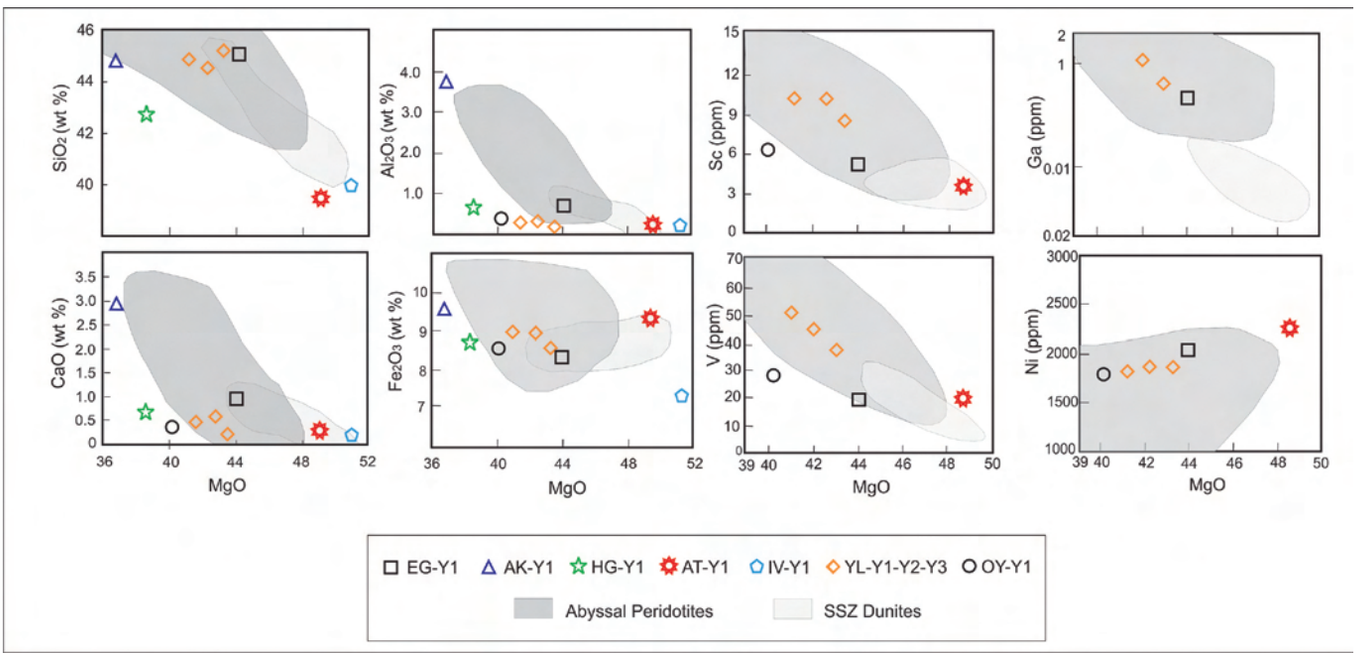

Fig. 6 - Variation of oxides and trace elements againts MgO (wt%) in the mantle peridotites (abyssal and SSZ fields are from Niu et al. (1997), Parkinson and Pearce (1998) and Uysal et al. (2012).

AT and OY, have the lowest and the highest Cr_2O_3 concentrations, respectively. There is positive correlation of Fe_2O_3 (r: 0.80), V (r: 0.45) and Co (r: 0.50) with Cr_2O_3 whereas negative correlations of SiO_2 (r: -0.83), MgO (r: -0.78) and Ni (r: -0.50) with Cr_2O_3 are clearly observed (Fig. 7).

Bulk concentrations of platinum group element (PGE) range between 52.4 and 114 ppb (ave. 92 ppb), lower than those in other significant chromite deposits (ave. 166-280 ppb) in Turkey (Table 6, Uysal et al., 2010). Chondrite normalized PGE patterns are shown in Fig. 8. All the chromitite samples display Os-Ir-Ru (Iridium group; IPGE) enrichments over Rh-Pt-Pd (Palladium group; PPGE) concentrations coupled with slightly positive Ru anomaly. While the chromitite sample from the AK mine shows the most enriched pattern, the sample from IV mine exhibits the least enriched pattern among all the deposits. Additionally, the values of Pt and Pd are under the detection limits (< 10 ppb). The Pd/Ir ratios are mostly lower than 1 for the chromitites. The Ir values range between 4.4-28 ppb (generally higher than 10 ppb). Moreover, the investigated chromitites display patterns similar to the mantle-hosted ophiolitic chromitites worldwide (Fig. 8; Uysal et al., 2005; Dönmez et al., 2014).

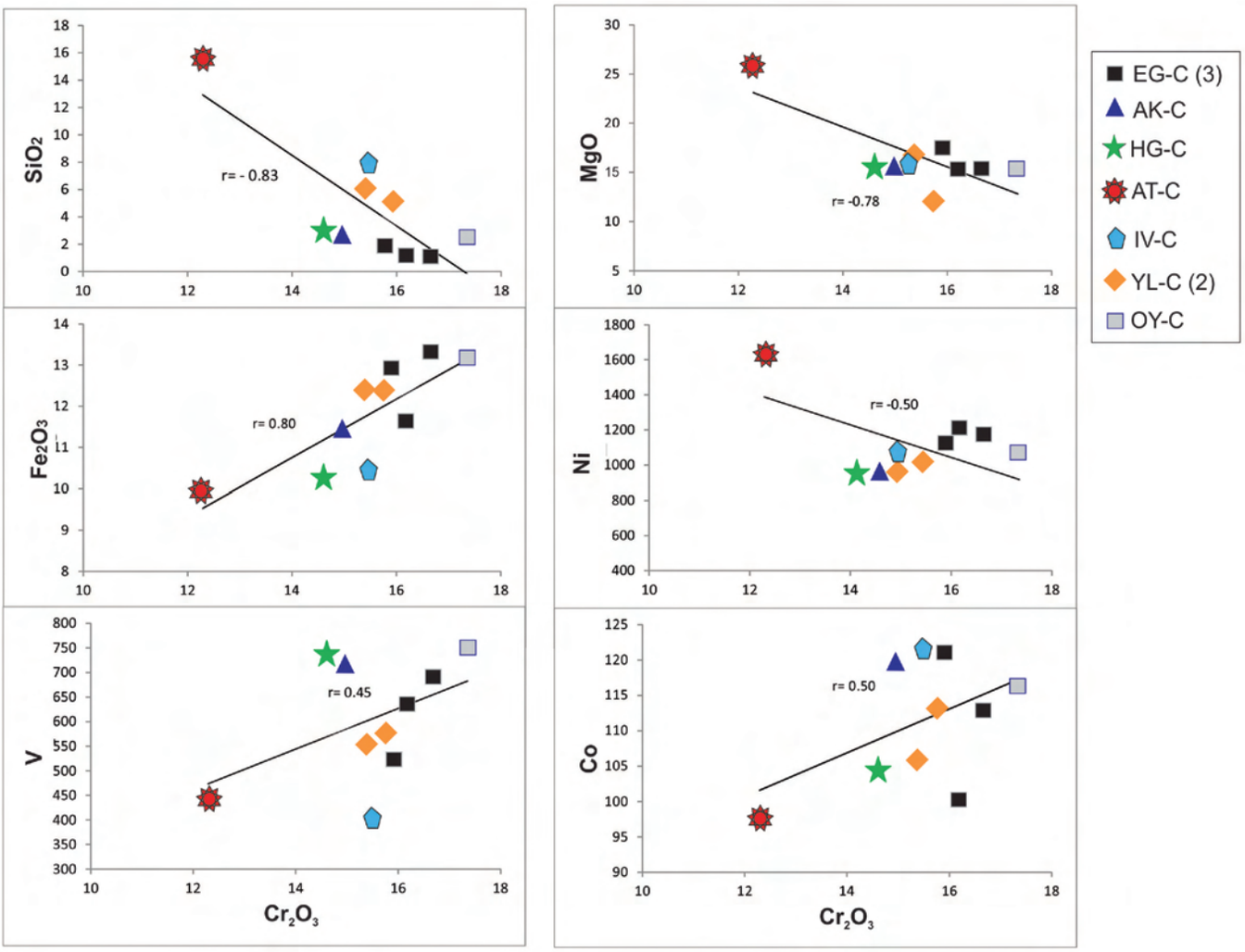

Fig. 7 - Variation diagrams for the chromitites.

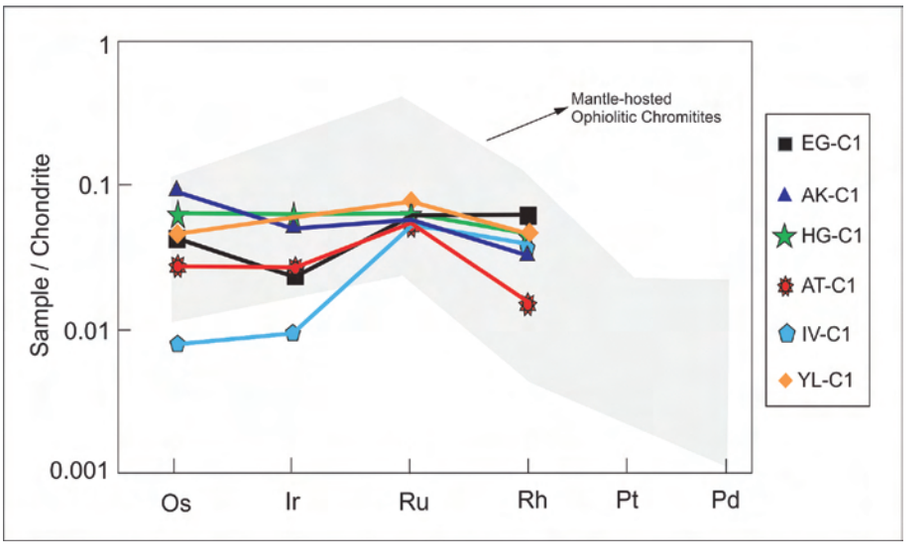

Fig. 8 - Chrondrite normalized PGE patterns of chromites (field of mantle-hosted ophiolitic complexes taken from Dönmez et al., 2014).

Table 6 - PGE data of the chromitites.

Sample	EG-C1	AK-C1	HG-C1	AT-C1	IV-C1	YL-C1	RDL (ppb)
Au	3.3	11.0	6.0	2.2	3.5	9.5	0.5
Ir	25.0	26.0	28.0	12.0	4.4	27.0	0.2
Os	21.0	41.0	31.0	14.0	4.0	23.0	1.0
Pd	<10	<10	<10	<10	<10	<10	10.0
Pt	<10	<10	<10	<10	<10	<10	10.0
Rh	8.0	4.0	6.0	2.0	5.0	6.0	1.0
Ru	42.0	43.0	46.0	40.0	39.0	55.0	10.0

RDL = Reportable Detection Limit.

DISCUSSION

Chemical variability of the mantle peridotites and inferences on their genesis

Low Na content of clinopyroxenes is consistent with a suboceanic mantle derivation. However, the secondary clinopyroxenes display higher Na values than the primary clinopyroxenes (Fig. 9a). The narrow range of Mg# and NiO (0.24-0.41 wt%) values in the olivine are similar to those from abyssal and fore-arc peridotites (Fig. 9b). The variations of TiO_2 againts Mg# in the clinopyroxenes mainly correspond to transitional compositions between fore-arc and abyssal peridotites; in particular, the higher TiO_2 contents of secondary clinopyroxenes are more akin to those from abyssal peridotites (Fig. 9c). The Al_2O_3 and Mg# values of orthopyroxenes show similarities to those of forearc peridotites (Fig. 9d). While the spinels from the clinopyroxene rich peridotites mostly plot into the abyssal peridotites, the spinels from the clinopyroxene poor peridotites plot in the field of fore-arc peridotites (Fig. 9e). Higher Cr# values in spinels coupled with relatively low Mg# values in olivine are commonly found in supra-subduction zone related peridotites (Fig. 9f). In Fig. 10a, the clinopyroxenes of peridotites plot in the fields of fore-arc and abyssal peridotites which is consistent with a typical back arc basin environment. Interaction between fore-arc peridotites and Ti rich melts (Fig. 10b) is supported by the composition of the secondary clinopyroxenes. In addition to the silicate mineral chemistry from the peridotites, the compositions of chromian spinels in the chromitites indicate a podiform type (Fig. 11a). This result is also corroborated by the presence of laurite in the chromitites. The low Al_2O_3 (< 20 wt%) and TiO_2 (< 0.3 wt%) concentrations of the spinels from these chromitites are consistent with a supra-subduction zone setting (Fig. 11b).

In summary, the studied peridotites display characteristics transitional between fore-arc and abyssal peridotites (Fig. 9) which may indicate derivation from a typical back arc basin environment (e.g., Bédard et al., 2009). Primary clinopyroxenes with low Al_2O_3 contents (0.73-1.87 wt%) coexisting with Cr-rich spinels (Cr# = 39-77) testify the depleted character of the peridotites. Such chemical features are consistent with high degree of partial melting (Fig. 9e; 18-31%), characteristics of subduction-related peridotites (Parkinson and Pearce, 1998; Pearce et al., 2000). Such high degrees of melting may be promoted by addition of H_2O-rich fluids (Davies and Bickle, 1991; Stolper and Newman, 1994; Taylor and Martinez, 2003; Langmuir et al., 2006).

These very low proportions of primary clinopyroxene indicate a strong depletion of the peridotites. Nevertheless, the chemical composition of secondary clinopyroxenes and TiO_2 enrichment of some coexisting Cr-rich spinels (TiO_2 up to 0.4 wt%) are in contrast with the highly residual character of the peridotites. These results suggest that melt extraction was followed by enrichment processes (refertilization) in a supra-subduction zone rather than a simple melt extraction in a mid-ocean environment (Saka et al., 2014). In other words, interaction between TiO_2 rich melts and previously depleted peridotites may have produced TiO_2 enrichments in the residual high Cr# spinels (Pearce et al., 2000; Choi et al., 2008) and enrichments in Ti, Al and Na in the secondary clinopyroxenes. These geochemical signatures are consistent with a back arc basin environment (Fig. 10).

The mantle peridotites mainly plot below the mantle array in the MgO/SiO_2 vs Al_2O_3/SiO_2 diagram (Fig. 5). This is most likely related to seafloor hydrothermal alteration (Snow and Dick, 1995; Niu, 2004; Uysal et al., 2012). Conversely, two dunite samples (IV and AT) plot above the terrestrial mantle array, which suggest interaction with olivine rich melts (Uysal et al., 2012) or higher degree of partial melting in a SSZ.

Whole rock and PGE geochemistry of the chromitites: implications on the origin

The relatively low Cr_2O_3 values of the chromitites may be interpreted as a result of limited melt-rock interaction in a intra-oceanic back arc basin. Remarkably, the lithospheric mantle is thinner in a back arc basin than a subduction zone due to spreading. Therefore, the degree of interaction between the mantle rocks and rising melts will be lower compared to a subduction zone (Zhou and Robinson, 1997).

The low PGE concentrations may be caused by lack of sulfur saturation during the early stage of their crystallization (Garuti and Zaccarini, 1997; Uysal et al., 2005) or by secondary processes (weathering, hydrothermal activity, serpentinization, metamorphism: e.g., Augé and Legendre, 1994; Prichard et al., 1986; Thalhammer et al., 1990; Zaccarini et al., 2005). The petrographic and EPMA evidences, showing well preservation of the PGM within the chromite crystals, rule out modification of PGE distribution by secondary processes. Therefore, low PGE concentrations in the chromitites could be related to primary magmatic features closely linked to the tectonic setting. Previous studies on chromitites have shown that Al-rich chromitites from spreading zones are characterized by low PGE contents

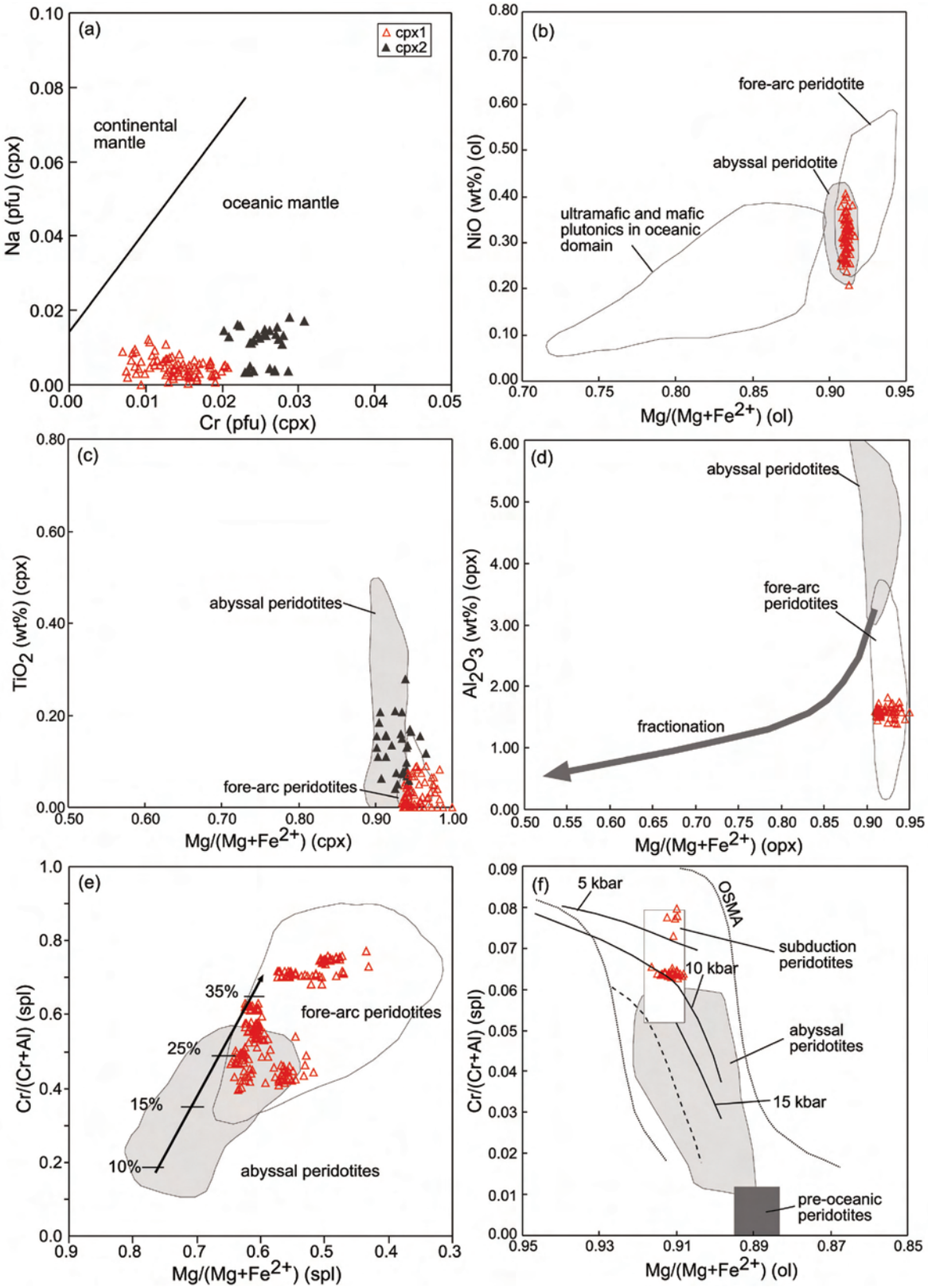

Fig. 9 - Variation of, (a) Na (pfu) againts Cr (pfu) in clinopyroxene (oceanic and continental mantle division is from Konrprobst et al., 1981), (b) NiO vs. Mg/(Mg + Fe^{2+}) in olivine (fields showing fore-arc and abyssal peridotites and ultramafic-mafic plutons are from Bédard et al., 2009 and references therein), (c) TiO_2 vs. Mg/(Mg + Fe^{2+}) in clinopyroxene (fields of abyssal and fore-arc peridotites are from Bédard et al., 2009 and references therein), (d) Al_2O_3 vs. Mg/(Mg + Fe^{2+}) in orthopyroxene (fields of abyssal and fore-arc peridotite are from Bédard et al., 2009 and references therein), (e) Cr/(Cr + Al) vs. Mg/(Mg + Fe^{2+}) for chromian spinels of the peridotites (fields of abyssal and fore-arc peridotites are from Bédard et al., 2009 and references therein, and wet partial melting trend is from Hirose and Kawamoto, 1995), (f) subduction related origin of the studied peridotites based on variation between Cr# of spinel and Mg# of olivine (olivine-spinel mantle array (OSMA) and field of abyssal peridotites are from Arai, 1994, fields of pre-oceanic and subduction peridotites are from Bonatti and Michael, 1989, pressure trends of 5 and 10 kbars are from Sobolev and Batanoba, 1995 and 15 kbar trend is from Jaques and Green, 1980).

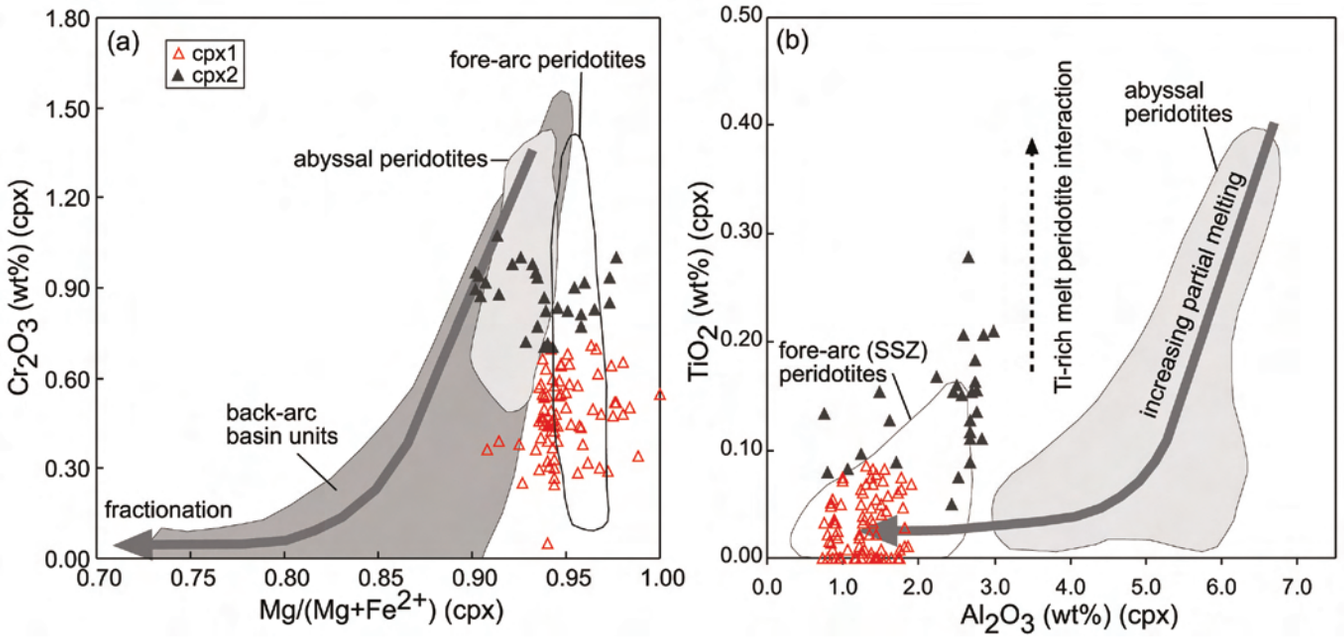

Fig. 10 - Variation of, (a) Cr_2O_3 with Mg Mg/(Mg+Fe^{2+}) in clinopyroxene (fields of abyssal and fore-arc peridotites, and back-arc basin units are from Bédard et al., 2009 and references therein), (b) TiO_2 with Al_2O_3 in clinopyroxene (fields of abyssal and fore-arc peridotites are from Hébert et al., 1990, Johnson et al., 1990, Ishii et al., 1992).

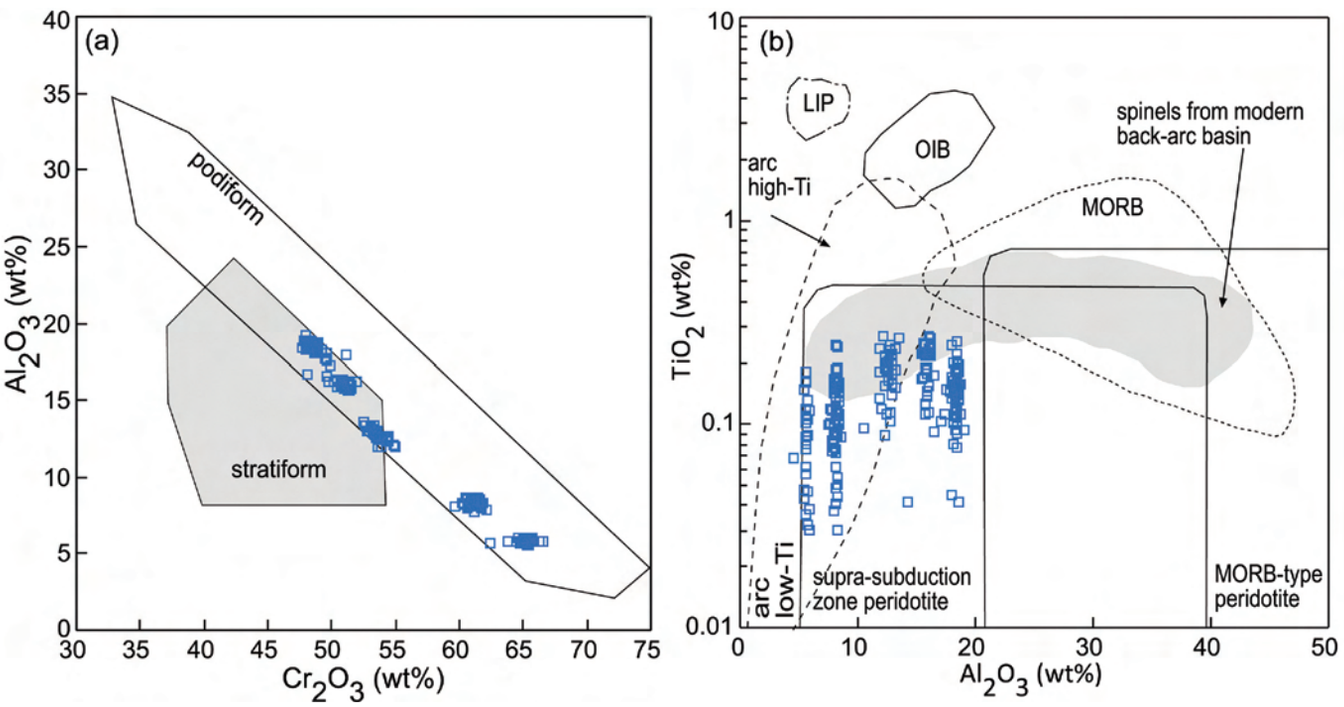

Fig. 11 - Compositional variations of chromian spinel of the chromitites: (a) Al_2O_3 with Cr_2O_3 (podiform and stratiform fields are Bonavia et al., 1993), (b) TiO_2 with Al_2O_3 (tectonic setting fields from Kamenetsky et al., 2001, LIP- large igneous province, OIB- ocean island basalt, MORB- mid-ocean basalt).

(e.g., Ahmed and Arai, 2003; Gervilla et al., 2005). These concentrations are the lowest among the other chromitite deposits in Turkey which were reported by Uysal et al. (2010). The chondrite-normalized PGE patterns display trends similar to those of mantle hosted ophiolitic chromitites (Fig. 8). These chromitites can be characterized by high IPGE/PPGE ratios, a typical feature of podiform chromitites (Zhou et al., 1996). The very low Pd contents (under detection limit)/Ir ratios may be conceively related to a depleted mantle source within a back arc basin (see Garuti et al., 1997).

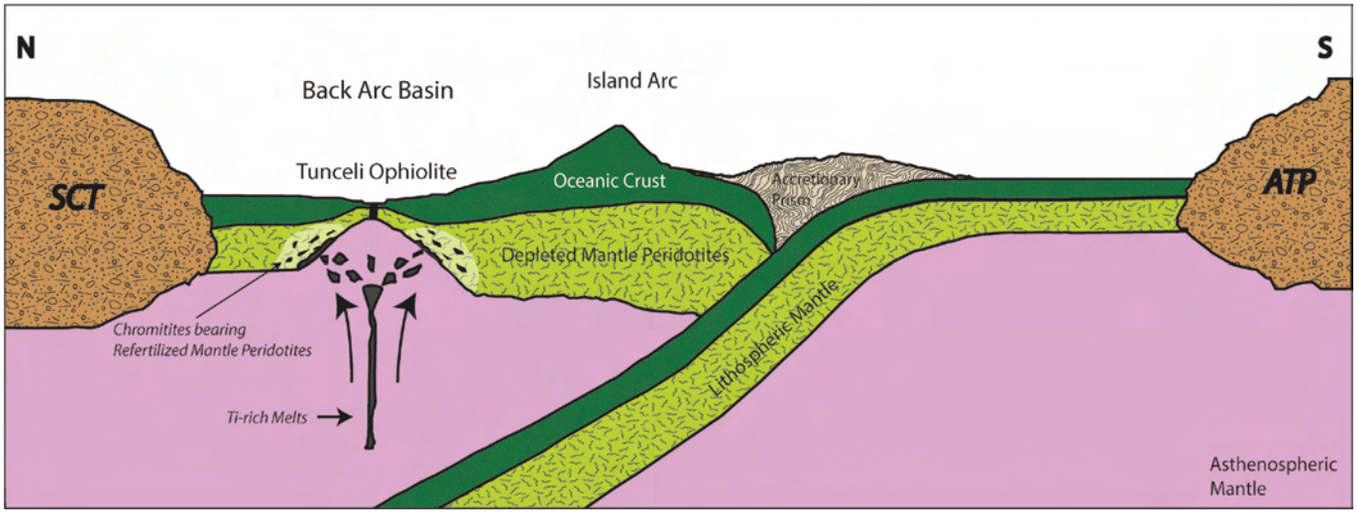

Fig. 12 - Simplified geodynamic model illustrating northward subduction of northern branch of Neotethyan and tectonic setting of the Tunceli Ophiolite (ATP- Anatolide-Tauride Platform; SCT- Sakarya Composite Terrane).

An overall approach to the geotectonic setting

There is still no consensus in relation to the formation of podiform chromitites associated with mantle peridotites in the literature. It is mostly accepted that these rocks were formed in a subduction zone or in a back arc basin environment (e.g., Zhou and Robinson, 1997; Zaccarini et al., 2011). The mantle peridotites from the Tunceli Ophiolite display both depleted and refertilized characteristics. Refertilization was likely due to interaction of Ti-rich melts with depleted peridotites. This inference is supported by the presence of secondary clinopyroxene with high Ti content associated with refractory spinel enriched in Ti. These results may be caused by rising of these melts in a spreading back arc basin. To sum up, the mantle peridotites of the Tunceli Ophiolite exhibit the signatures of a typical back arc basin which may have been developed in a supra-subduction zone (Fig. 12).

CONCLUDING REMARKS

The geochemical data of the mantle peridotites and chromitites indicate that the Tunceli Ophiolite may have formed in an intra-oceanic back arc basin. Similar conclusions have been previously reached on the basis of geochemical signatures of magmatic rocks within this ophiolite (Çimen et al., 2014). In general, the mineral chemistry results including olivine, pyroxene and spinel minerals display the geochemical characteristic of fore-arc and abyssal peridotites. Moreover, the presence of secondary clinopyroxenes and high-Ti spinel indicate the interaction between depleted peridotites and Ti rich melt that have caused a refertilization process. Overall, the consistent geochemical and mineral chemistry data from these mantle peridotites, chromitites and magmatic rocks within the Tunceli Ophiolites are consistent with origin in a intra-oceanic back-arc basin which should have been active through closure of northern branch of the Neotethyan ocean.

ACKNOWLEDGEMENTS

This research was supported by the Tunceli University with a project number of MFTUB013-09. Ali Önal is thanked for assistance during the field studies. The authors gratefully acknowledge Alessandra Montanini, Alessio Sanfilippo and Michele Marroni for their detailed and thoughtful comments, which scientifically improved the manuscript.

REFERENCES

Ahmed AH. and Arai S., 2003. Platinum-group minerals in podiform chromitites of the Oman ophiolite. Can. Mineral., 41: 597-616.

Akbulut M., Pişkin Ö., Arai S., Özgenç I. and Minareci F., 2010. Base metal (BM) and platinum-group elements (PGE) mineralogy and geochemistry of the Elmaslar chromite deposit (Denizli, SW Turkey): implications for a local BM and PGE enrichment. Ofioliti, 35 (1): 1-20.

Aldanmaz E., Yalınız M.K., Güçtekin A. and Göncüoğlu M.C., 2008. Geochemical characteristics of mafic lavas from the Tethyan ophiolites in western Turkey: implications for heterogeneous source contribution during variable stages of ocean crust generation. Geol. Mag., 145: 37-54.

Arai S., 1994. Characterization of spinel peridotites by olivine-spinel compositional relationships: review and interpretation. Chem. Geol., 113, 191-204.

Augé T. and Legendre O., 1994. Platinum-group element oxides from the Pirogues ophiolitic mineralization, New Caledonia. Econ. Geol., 89: 1454-1468.

Barnes S.J. and Roader P.L., 2001. The range of spinel composition in terrestrial mafic and ultramafic rocks. J. Petrol., 42: 2279-2302.

Bédard É., Hébert R., Guilmette C., Lesage G., Wang C.S. and Dostal J., 2009. Petrology and geochemistry of the Saga and Sangsang ophiolitic massifs, Yarlung Zangbo Suture Zone, Southern Tibet: Evidence for an arc-back-arc origin. Lithos, 113: 48-67.

Bonatti E. and Michael P.J., 1989. Mantle peridotites from continental rifts to ocean basins to subduction zones. Earth Planet. Sci. Lett., 91: 297-311.

Bonavia F.F., Diella V. and Ferrario A., 1993. Precambrian podiform chromitites from Kenticha Hill, southern Ethiopia. Econ. Geol., 88: 198-202.

Bortolotti V., Chiari M., Marroni M., Pandolfi L., Principi G. and Saccani E., 2013. Geodynamic evolution of ophiolites from Albania and Greece (Dinaric-Hellenic belt): one, two, or more oceanic basins? Int. J. Earth Sci., 102: 783-811.

Çelik Ö.F., Marzoli A., Marschik R., Chiaradia M., Neubauer F. and Öz İ., 2011. Early-Middle Jurassic intra-oceanic subduction in the İzmir-Ankara-Erzincan Ocean, Northern Turkey. Tectonophysics, 509: 120-134.

Choi S.H., Shervais J.V. and Mukasa S.B., 2008. Supra-subduction and abyssal mantle peridotites of the coast range ophiolite. Contrib. Mineral. Petrol., 156: 551-576.

Çimen O., Sayit K., Göncüoğlu M.C., Öztüfekçi-Önal A. and Aktağ A., 2014. MORB and SSZ type mafic rocks from the eastern part of the Ankara-Erzincan-Sevan-Akera Suture Belt: Preliminary geochemical data. Goldschmidt, 428 pp.

Davies J.H. and Bickle M.J., 1991. A physical model for the volume and composition of melt produced by hydrous fluxing above subduction zones. Philos. T. R. Soc., 335: 355-364.

Dilek Y. and Thy P., 2006. Age and petrogenesis of plagiogranite intrusion in the Ankara Mélange, central Turkey. Isl. Arc, 15: 44-57.

Dönmez C., Keskin S., Günay K., Çolakoğlu A.O., Çiftçi Y., Uysal İ., Türkel A. and Yıldırım Y., 2014. Chromite and PGE geochemistry of the Elekdağ Ophiolite (Kastamonu, Northern Turkey): Implications for deep magmatic processes in a supra-subduction zone setting. Ore Geol. Rev., 57: 216-228.

Droop G.T.R., 1987. A general equation for estimating Fe^{3+} concentrations in ferromagnesian silicates and oxides from microprobe analysis, using stoichiometric criteria. Min. Mag., 51: 431-437.

Eyüboğlu Y., Bektas O. and Pul D., 2007. Mid-Cretaceous olistostromal ophiolitic mélange developed in the back-arc basin of the eastern Pontide magmatic arc, northeast Turkey. International Geology Review, 49: 1103-1126.

Floyd P.A., 1993. Geochemical discrimination and petrogenesis of alkalic basalt sequences in part of the Ankara Mélange, central Turkey. J. Geol. Soc. London, 150: 541-550.

Floyd P.A. and Winchester J.A., 1978. Identification and discrimination of altered and metamorphosed volcanic rocks using immobile elements. Chem. Geol., 21: 291-306.

Floyd P.A., Winchester J.A., Seston R., Kryza R. and Crowley Q.G., 2000. Review of geochemical variation in Lower Palaezoic metabasites from the NE Bohemian Massif; intracratonic rifting and plume ridge interaction. In: W. Franke, V. Haak, O. Oncken and D. Tanner (Eds.), Orogenic processes: Quantifications and modeling in the Variscan Belt. Geol. Soc. London Spec. Publ., 179: 155-174.

Garuti G. and Zaccarini F., 1997. *In situ* alteration of platinum group minerals at low temperature: evidence from serpentinized and weathered chromitite of the Vourinos complex, Greece. Can. Mineral., 35: 611-626.

Garuti G., Fershtater G., Bea F., Montero P., Pushkarev E.V. and Zaccarini F., 1997. Platinum-group elements as petrological indicators in mafic-ultramafic complexes of the central and Southern Urals, preliminary results. Tectonophysics, 276: 181-194.

Garuti G., Pushkarev E.V., Thalhammer O.A.R. and Zaccarini F., 2012. Chromitites of the Urals (Part1): Overview of chromite mineral chemistry and geo-tectonic setting. Ofioliti, 37 (1): 27-53.

Gervilla F., Proenza J.A., Frei R., González-Jiménez J.M., Garrido C.J., Melgarejo J.C., Meibom A., Díaz-Martínez R. and Lavaut W., 2005. Distribution of platinum-group elements and Os isotopes in chromite ores from Mayarí-Baracoa Ophiolitic Belt (eastern Cuba). Contrib. Mineral. Petrol., 150: 589-607.

Ghazi J.M., Moazzem M., Rahghoshay M. and Moghadam H.S., 2011. The geodynamic setting of the Nain Ophiolites, Central Iran: Evidence from chromite spinels in the chromitites and associated rocks. Ofioliti, 36 (1): 59-76.

Göncüoğlu M.C., 2010. Introduction to the geology of Turkey: Geodynamic evolution of the pre-Alpine and Alpine Terranes. MTA, Special Issue, 69 pp.

Göncüoğlu M.C., Gürsu S., Tekin U.K. and Köksal S., 2008. New data on the evolution of the Neotethyan oceanic branches in Turkey: Late Jurassic ridge spreading in the Intrapontide branch. Ofioliti, 33: 53-164.

Göncüoğlu M.C., Kozlu H. and Dirik K., 1997. Pre-Alpine and Alpine terranes in Turkey: explanatory notes to the terrane map of Turkey. Ann. Géol. Pays. Hellén., 37: 515-536.

Göncüoğlu M.C., Turhan N., Sentürk K., Özcan A. and Uysal S., 2000. A geotraverse across NWTurkey: tectonic units of the Central Sakarya region and their tectonic evolution. In: E. Bozkurt, J.A. Winchester and J.D. Piper (Eds.), Tectonics and magmatism in Turkey and the surrounding area. Geol. Soc. London Spec. Publ., 173: 139-162.

Göncüoğlu M.C., Yalınız M.K. and Tekin U.K., 2006a. Geochemistry, tectono-magmatic discrimination and radiolarian ages of basic extrusives within the Izmir-Ankara Suture Belt (NW Turkey): Time constraints for the Neotethyan evolution. Ofioliti, 31: 25-38.

Göncüoğlu M.C., Yalınız M.K. and Tekin U.K., 2006b. Geochemical features and radiolarian ages of volcanic rocks from the Izmir-Ankara Suture Belt, western Turkey. Mesozoic ophiolite belts of the northern part of the Balkan Peninsula, Proceed., p. 41-44.

Green D.H., 1973. Experimental melting studies on a model upper mantle composition at high pressure under water-saturated and water-unsaturated conditions. Earth Planet. Sci. Lett., 19: 37-53.

Günay K. and Çolakoğlu A.Ç., 2011. Geochemical properties and platinum group element (PGE) contents of Eastern Turkey (Van Area) chromitite. Geol. Bull. Turkey, 54 (1-2): 1-24.

Hébert R., Adamson A.C. and Komor S.C., 1990. Metamorphic petrology of ODP 109, Hole 670A serpentinized peridotites: serpentinization processes at a slow spreading ridge environment. In: R. Detrick, J. Honnorez, W.B. Bryan and T. Juteau (Eds.), Proceed. O.D.P., Sci. Res., 106/109, p. 103-115.

Hirose K. and Kawamoto T., 1995. Hydrous partial melting of lherzolite at 1 Gpa: the effect of H_2O on the genesis of basaltic magmas. Earth Planet. Sci. Lett., 133: 463-473.

Ishii T., Robinson P.T., Maekawa H., and Fiske R., 1992. Petrological studies of peridotites from diapiric serpentinite seamounts in the Izu-Ogasawara-Mariana Forearc, Leg 125. In: O. Fryer, J.A. Pearce, L.B. Stokking et al. (Eds.), Proceed. O.D.P., Sci. Res., 125, p. 445-485.

Jaques A.L. and Green D.H., 1980. Anhydrous melting of peridotites at 0-15 kbar pressure and the genesis of tholeiitic basalts. Contrib. Miner. Petrol., 73: 287-310.

Johnson K.T.M., Dick H.J.B. and Shimizu N., 1990. Melting in the oceanic upper mantle: an ion microprobe study of diopsides in abyssal peridotites. J. Geophys. Res., 95: 2661-2678.

Kamenetsky V.S., Crawford A.J. and Meffre S., 2001. Factors controlling chemistry of magmatic spinel: an empirical study of associated olivine, Cr-spinel and melt inclusions from primitive rocks. J. Petrol., 42: 655-671.

Kornprobst J., Ohnenstetter D. and Ohnenstetter M., 1981. Na and Cr contents in cpx from peridotites: a possible discriminant between 'sub-continental' and 'sub-oceanic' mantle. Earth Planet. Sci. Lett., 53: 241-254.

Langmuir C.H., Bézos A., Escrig S. and Parman S.W., 2006. Chemical systematics and hydrous melting of the mantle in back-arc basins. In: D.M. Christie et al. (Eds.), Back-arc spreading systems: geological, biological, chemical and physical interactions. Geophys. Monogr. Ser., 166: 87-146.

McDonough W.F. and Sun S.S., 1995. The composition of the earth. Chem. Geol., 120: 223-253.

Montanini A., Tribuzio L. and Thirlwall M., 2012. Garnet clinopyroxenite layers from the mantle sequences of the Northern Apennine ophiolites (Italy): Evidence for recycling of crustal material. Earth Planet. Sci. Lett., 351-352: 171-181.

MTA (Mineral Research and Exploration General Directorate), 2008. Geology Report of J42-J43.

Niu Y., 2004. Bulk-rock major and trace element composition of abyssal peridotites, implications for mantle melting, melt extraction and post-melting processes beneath Mid-ocean Ridges. J. Petrol., 45: 2423-2458.

Niu Y., Langmuir C.H. and Kinzler R.J., 1997. The origin of abyssal peridotites: a new perspective. Earth Planet. Sci. Lett., 152: 251-265.

Okay A.I. and Sahintürk Ö., 1997. Geology of the Eastern Pontides, In: A.G. Robinson (Ed.), Regional and petroleum geology of the Black Sea and surrounding region: Am. Ass. Petr. Geol. Mem., 68: 291-311.

Okay A.I., Tüysüz O., Satır M., Özkan-Altıner S., Altıner D., Sherlock S. and Eren R.H., 2006. Cretaceous and Triassic subduction-accretion, high-pressure-low-temperature metamorphism, and continental growth in the Central Pontides, Turkey. G.S.A. Bull., 118: 1247-1269.

Önen A.P., 2003. Neotethyan ophiolitic rocks of the Anatolides of NW Turkey and comparison with Tauride ophiolites. J. Geol. Soc. London, 160: 947-962.

Önen A.P. and Hall R., 1993. Ophiolites and related metamorphic rocks from the Kütahya region, northwest Turkey. Geol. J., 28: 399-412.

Öztüfekçi-Önal A., Toksoy-Köksal F., Zaccarini F., Cimen O., Aktağ A. and Önal A., 2014. First description of platinum group minerals (PGMs) in ultramafic rocks of the Ovacık and Pülümür ophiolitic complex, Tunceli, Turkey. 11th EMAS Regional Workshop.

Parlak O., Çolakoğlu A., Dönmez C., Sayak H., Yıldırım N., Türkel A. and Odabaşı İ., 2012. Geochemistry and tectonic significance of ophiolites along the Ankara-Erzincan Suture Zone in northeastern Anatolia. In: A.H.F. Robertson, O. Parlak and U.C. Ünlügenç (Eds.), 2012. Geol. Soc. London Spec. Publ., 372 (1): 75-106.

Parkinson I.J. and Pearce J.A., 1998. Peridotites from the Izu-Bonin-Mariana Forearc (ODP Leg 125), evidence for mantle melting and melt-mantle interaction in a suprasubduction zone setting. J. Petrol., 39: 1577-1618.

Pearce J.A. and Cann J.R., 1973. Tectonic setting of basic volcanic rocks determined using trace element analyses. Earth Planet. Sci. Lett., 19 (2): 290-300.

Pearce J.A. and Norry M., 1979. Petrogenetic implications of Ti, Zr, Y and Nb variations in volcanic rocks. Contrib. Mineral. Petrol., 69: 33-47.

Pearce J.A., Barker P.F., Edwards S.J., Parkinson I.J. and Leat P.T., 2000. Geochemistry and tectonic significance of peridotites from South Sandwich arc-basin system, South Atlantic. Contrib. Mineral. Petrol., 139: 36-53.

Prichard H., Neary C. and Potts PJ., 1986. Platinum group minerals in the Shetland ophiolite. In M.J. Gallagher et al. (Eds), Metallogeny of basic and ultrabasic rocks. Inst Min. Metall. London, p. 395-414.

Rice S.P., Robertson A.H.F. and Ustaömer T., 2006. Late Cretaceous-Early Cenozoic tectonic evolution of the Eurasian active margin in the Central and Eastern Pontides, northern Turkey. In: A.H.F. Robertson (Ed.), Tectonic development of the Eastern Mediterranean Region. Geol. Soc. London Spec. Publ., 260: 413-445.

Robertson A.H.F., Parlak O., Ustaömer T., Taslı K., İnan N., Dumitrica P. and Karaoğlan F., 2013. Subduction, ophiolite genesis and collision history of Tethys adjacent to the Eurasian continental margin: new evidence from the Eastern Pontides, Turkey. Geodyn. Acta, 26: 230-293.

Saccani E., Allahyari K., Beccaluva L. and Bianchini G., 2013. Geochemistry and petrology of the Kermanshah ophiolites (Iran): Implication for the interaction between passive rifting, oceanic accretion, and plume-components in the Southern Neo-Tethys Ocean. Gondwana Research, 24: 392-411.

Saccani E. and Tassinari R., 2015. The role and MORB and SSZ magma-types in the formation of Jurassic ultramafic cumulates in the Mırdıta Ophiolites (Albania) as deduced from chromian spinel and olivine e chemistry. Ofioliti, 40 (1): 37-56.

Saka S., Uysal İ., Akmaz RM., Kaliwoda M. and Hochleitner R., 2014. The effects of partial melting, melt-mantle interaction and fractionation on ophiolite generation: Constraints from the Late Cretaceous Pozantı-Karsantı ophiolite, southern Turkey. Lithos, 202-203: 300-316.

Sanfilippo A., Tribuzio R., Tiepolo M. and Berno D., 2015. Reactive flow as dominant evolution process in the lowermost oceanic crust: evidence from olivine of the Pineto ophiolite (Corsica). Contrib. Mineral. Petrol., 170: 38.

Snow J.E. and Dick H.J.B., 1995. Pervasive magnesium loss by marine weathering of peridotite. Geochim. Cosmochim. Acta, 59: 4219-4235.

Sobolev A.V. and Batanova V.G., 1995. Mantle lherzolites of the Troodos ophiolite complex, Cyprus: clinopyroxene geochemistry. Petrology, 3: 440-448.

Sobolev N.V. and Logvinova A.M., 2005. Significance of accessory chrome spinel in identifying serpentinite paragenesis. Int. Geol. Rev., 47: 58-64.

Stolper E. and Newman S., 1994. The role of water in the petrogenesis of Mariana trough magmas. Earth Planet. Sci. Lett., 121: 293-325.

Şengör A.M.C. and Yılmaz Y., 1981. Tethyan evolution of Turkey: A plate tectonic approach. Tectonophysics, 75: 181-241.

Taylor B. and Martinez F., 2003. Back-arc basin basalt systematics. Earth Planet. Sci. Lett., 210: 481-497.

Thalhammer O.A.R., Prochaska W. and Mühlhans H.W., 1990. Solid inclusions in chromespinels and platinum group element concentrations from the Hochgrössen and Krabath ultramafic massif (Austria). Contrib. Mineral. Petrol., 105: 66-80.

Toksoy-Köksal F., Göncüoglu M.C. and Yaliniz M.K., 2001. Petrology of the Kurancali Phlogopitic Metagabbro: An island arc-type ophiolitic sliver in the Central Anatolian Crystalline Complex, Turkey. Int. Geol. Rev., 43: 624-639.

Toksoy-Köksal F., Oberhansli R. and Göncüoğlu M.C., 2009. Hydrous aluminosilicate metasomatism in an intra-oceanic subduction zone: Implications from the Kurancali (Turkey) ultramafic-mafic cumulates within the Alpine Neotethys Ocean. Miner. Petrol., 95: 273-290.

Topuz G., Çelik O.F., Şengör A.M.C., Altıntaş I.E., Zack T., Rolland Y. and Barth M., 2013. Jurassic ophiolite formation and emplacement as backstop to a subduction-accretion complex in northeast Turkey, the Refahiye ophiolite, and relation to the Balkan ophiolites. Am. J. Sci., 313: 1054-1087.

Uçurum A. and Koptagel O., 2006. Main-component geochemistry and platinum-group element potential of Turkish chromite deposits, with emphasis on the Mugla area. Int. Geol. Rev., 48: 241-254.

Uçurum A., Lechler P.J. and Larson L.T., 2000. Platinum-group element distribution in chromite ores from ophiolite complexes, Western Turkey. Trans. Inst. Min. Metall. Sect. B-Appl. Earth. Sci., 109: 112-120.

Uysal I., Ersoy E.Y., Dilek Y., Escaloya M., Sarıfakıoğlu E., Saka S. and Hirata T., 2015. Depletion and refertilization of the Tethyan oceanic upper mantle as revealed by the early Jurassic Refahiye ophiolite, NE Anatolia-Turkey. Gondw. Res., 27: 594-611.

Uysal I., Ersoy E.Y., Karslı O., Dilek Y., Sadıklar M.B., Ottley C.J., Tiepolo M. and Meisel T., 2012. Coexistence of abyssal and ultra-depleted SSZ type mantle peridotites in a Neo-Tethyan ophiolite in SW Turkey: constraints from mineral composition, whole-rock geochemistry (major-trace-REE-PGE), and Re-Os isotope systematics. Lithos, 132-133: 50-69.

Uysal I., Kaliwoda M., Karslı O., Tarkian M., Sadıklar M.B. and Ottley C.J., 2007. Compositional variations in whole rock and coexisting phases with partial melting and melt-peridotite interaction in an upper mantle section from the Ortaca Area, southwestern Turkey. Can. Mineral., 45: 1471-1493.

Uysal I., Sadıklar M.B., Tarkian M., Karslı O. and Aydın F., 2005. Mineralogy and composition of the chromitites and their platinum-group minerals from Ortaca (Muğla- SW Turkey): evidence for ophiolitic chromitite genesis. Miner. Petrol., 83: 219-242.

Uysal I., Sadıklar M.B., Zaccarini F., Garuti G., Tarkian M. and Meisel T., 2010. Cr-PGE mineralization in the Turkish ophiolites: The state of the art. 11th Intern. Platinium Symp. Ontario Geol. Survey. Miscel. Release-Data, 269.

Uysal I., Tarkian M., Sadiklar M.B., Zaccarini F., Meisel T., Garuti G. and Heidrich S., 2009. Petrology of high-Cr and high-Al ophiolitic chromitites from the Muğla, SW Turkey: implications from composition of chromite, solid inclusions of platinum group mineral (PGM), silicate, and base-metal mineral (BMM), and Os-isotope geochemistry. Contrib. Mineral. Petrol., 158: 659-674.

Yalınız M.K., Floyd P.A. and Göncüoğlu M.C., 2000. Geochemistry of volcanic rocks from the Çiçekdağı ophiolite, central anatolia, Turkey, and their inferred tectonic setting within the Northern branch of the neotethyan ocean. In: E. Bozkurt, J.A. Winchester and J.D.A. Piper (Eds.), Tectonics and magmatism in Turkey and the surrounding area. Geol. Soc. London Spec. Publ., 173: 171-182.

Yılmaz Y., Tüysüz O., Yiğitnaş E., Genc C.S. and Şengör AMC., 1997. Geology and tectonic evolution of the Pontides. In: A.G. Robinson (Ed.), Regional and petroleum geology of the Black Sea and surrounding region. Am. Ass. Petrol. Geol. Mem., 68: 183-226.

Zaccarini F., Garuti G., Proenza J.A., Campos L., Thalhammer O.A.R., Aiglsperger T. and Lewis J., 2011. Chromite and platinum-group-elements mineralization in the Santa Elena ophiolitic ultramafic nappe (Costa Rica): geodynamic implications. Geol. Acta, 9 (3): 407-423.

Zaccarini F., Proenza A.J., Ortega-Gutierrez F. and Garuti G., 2005. Platinum group minerals in ophiolitic chromitites from Tehuitzingo (Acatlan complex, southern Mexico): implications for post-magmatic modification. Mineral. Petrol., 84: 147-168.

Zhou M.F. and Robinson P.T., 1997. Origin and tectonic environment of podiform chromite deposits. Econ. Geol., 92: 259-262.

Zhou M.F., Robinson P.T., Malpas J. and Li Z., 1996. Podifrom chromitites in the Luobusa ophiolite (southern Tibet): implications for melt-rock interaction and chromite segregation in the upper mantle. J. Petrol., 37: 3-21.

Received, November 20, 2015
Accepted, May 7, 2016